

THS MICHIGAN STATE UNIVERSITY LIBRARIES

22722043

THESE

LIBRARY Michigan State University

This is to certify that the

thesis entitled

METHODS OF PARTICLE DISCRIMINATION

FOR NUCLEAR SCATTERING EXPERIMENTS

presented by

PHILIP BRIEN UGOROWSKI

has been accepted towards fulfillment of the requirements for

Master's degree in Physics

Date___2/22/89

O-7639

MSU is an Affirmative Action/Equal Opportunity Institution

Sary D. Westall

Major professor



RETURNING MATERIALS:

Place in book drop to remove this checkout from your record. FINES will be charged if book is returned after the date stamped below.

METHODS OF PARTICLE DISCRIMINATION FOR NUCLEAR SCATTERING EXPERIMENTS

BY

Philip Brien Ugorowski

A THESIS

Submitted to
Michigan State University
in partial fulfillment of the requirements
for the degree of

MASTER OF SCIENCE

Department of Physics and Astronomy

1989

ABSTRACT

METHODS OF PARTICLE DISCRIMINATION FOR NUCLEAR SCATTERING EXPERIMENTS

By

Philip Brien Ugorowski

When a nucleus-nucleus collision results in the ejection of a nuclear fragment, the angle of flight and the energy of the particle can be determined using a detector containing a crystal scintillator, which absorbs all of the particles' kinetic energy (E). The present method of determining the particles' identity involves adding a thin slice of some scintillating material to the front of the detector to determine dE/dx, the energy lost per unit length in this material. After many events, a graph of dE/dx vs. E will show a band structure, requiring the experimenter interested in a particular isotope to spend time recording all particle events. It was the aim of this project to develop a method to determine the identity of any single particle, solely through analysis of its' dE/dx and E characteristics, using digitization and zero-cross techniques.

Copyright by PHILIP BRIEN UGOROWSKI 1989

TABLE OF CONTENTS

List of Figures	٠,
Introduction	. 1
Experimental Approach	. 8
Conclusions	40
Bibliography	41
General References	42

LIST OF FIGURES

Fig.	1Detector and Photomultiplier Tube3
Fig.	2Photomultiplier Anode Current vs. Time3
Fig.	3Comparison of Fast and Slow Gates4
Fig.	4(a)Fast Gate vs. Slow Gate, CsI4
Fig.	4(b)Fast Gate vs. Slow Gate, BaF ₂ 5
Fig.	4(c)Fast Gate vs. Slow Gate, NaI5
Fig.	4(d)Fast Gate vs. Slow Gate, Plastic6
Fig.	5Digitization of Single Pulse,
Fig.	6(a)E (Slow Gate) vs. t9
Fig.	6(b)Fast Gate vs. t9
Fig.	7Channel of Best Resolution, E vs. t
Fig.	9(a)Si vs. E, BaF ₂ 13
Fig.	9(b)Si vs. E, CsI
Fig.	9(c)Si vs. E, NaI, showing Li contour14
Fig.	9(d)Si vs. E, Plastic14
Fig.	10(a)CsI Channel of Best Resolution;
Fig.	10(b)CsI Channel of Best Resolution; ³ He, ⁴ He
Fig.	10(c)CsI Channel of Best Resolution; 4He, 6He16
Fig.	10(d)CsI Channel of Best Resolution; ⁶ Li, ⁷ Li

Fig.	11Pulser Calibration of MeV/Channel18
Fig.	12(a)dE/dx (Si) vs. E, CsI, ³ He contour
Fig.	12(b)Power Law Fit for ³ He Isotope19
Fig.	13(a)E _{calc} vs. E, CsI, Calculated for Z=1, A=122
Fig.	13(b)Channel of Best Resolution, CsI, Z=1, A=122
Fig.	14(a)E _{calc} vs. E, CsI, Calculated for Z=1, A=223
Fig.	14(b)Channel of Best Resolution, CsI, Z=1, A=223
Fig.	15(a)E _{calc} vs. E, CsI, Calculated for Z=1, A=324
Fig.	15(b)Channel of Best Resolution, CsI, Z=1, A=324
Fig.	16(a)E _{calc} vs. E, CsI, Calculated for Z=2, A=325
Fig.	16(b)Channel of Best Resolution, CsI, Z=2, A=325
Fig.	17(a)E _{calc} vs. E, CsI, Calculated for Z=2, A=426
Fig.	17(b)Channel of Best Resolution, CsI, Z=2, A=426
Fig.	18(a)E _{calc} vs. E, CsI, Calculated for Z=2, A=627
Fig.	18(b)Channel of Best Resolution, CsI, Z=2, A=627
Fig.	19(a)E _{calc} vs. E, CsI, Calculated for Z=3, A=628
Fig.	19(b)Channel of Best Resolution, CsI, Z=3, A=628
Fig.	20(a)E _{calc} vs. E, CsI, Calculated for Z=3, A=729
Fig.	20(b)Channel of Best Resolution, CsI, Z=3, A=729
Fig.	21(a)E _{calc} vs. E, CsI, Calculated for Z=3, A=830
Fig.	21(b)Channel of Best Resolution, CsI, Z=3, A=830
Fig.	22(a)E _{calc} vs. E, BaF ₂ , Calculated for Z=1, A=131
Fig.	22(b)Channel of Best Resolution, BaF ₂ , Z=1, A=131

Fig.	23(a)E _{calc} vs. E, BaF ₂ , Calculated for Z=1, A=232
Fig.	23(b)Channel of Best Resolution, BaF ₂ , Z=1, A=232
Fig.	24(a)E _{calc} vs. E, BaF ₂ , Calculated for Z=1, A=333
Fig.	24(b)Channel of Best Resolution, BaF ₂ , Z=1, A=333
Fig.	25(a)E _{calc} vs. E, BaF ₂ , Calculated for Z=2, A=334
Fig.	25(b)Channel of Best Resolution, BaF ₂ , Z=2, A=334
Fig.	26(a)E _{calc} vs E, BaF ₂ , Calculated for Z=2, A=435
Fig.	26(b) Channel of Best Resolution, BaF ₂ , Z=2, A=435
Fig.	27(a)E _{calc} vs E, BaF ₂ , Calculated for Z=2, A=636
Fig.	27(b)Channel of Best Resolution, BaF ₂ , Z=2, A=636
Fig.	28(a)E _{calc} vs E, BaF ₂ , Calculated for Z=3, A=637
Fig.	28(b)Channel of Best Resolution, BaF ₂ , Z=3, A=637
Fig.	29(a)E _{calc} vs Zerocross Time, CsI
Fig.	29(b)Projection of E _{calc} vs. Zerocross Time onto Time Axis.38
Fig.	30(a) E _{calc} vs. Fast Gate, CsI
Fig.	30(b)E _{calc} vs. Slow Gate39

INTRODUCTION

One of the principal investigative methods used to study the nucleus of the atom and the strong (nuclear) force is the method of scattering experiments. At the National Superconducting Cyclotron Laboratory, atoms of a particular element are ionized, accelerated and directed at a target of another element containing stationary atomic nuclei. Depending on the energy of the collision, the nuclei may scatter elastically, inelastically, or shatter into fragments. These different collision modes are prominent at different collision energies, and the actual event may be some combination of these. When a nucleus-nucleus collision results in the ejection of a nuclear fragment, the angle of flight and the energy of the particle can be determined. Note that the term "fragment" is used loosely -- the fragment may have formed from an inelastic collision and may therefore have a greater mass than either of the two original nuclei. The detector can be positioned within the scattering chamber to find the angle of flight. To measure the energy of the fragment, the detector must be thick enough to absorb all of the particle's kinetic energy (E), stopping the particle completely. These detectors may be of several types. The ones used here contained various inorganic crystalline scintillating compounds, specifically cesium iodide, sodium iodide, barium fluoride, and organic scintillators. There are several ways the particle's energy can be dissipated in the crystal along the path of its flight. One way is by the excitation of some bound electrons in the crystal. After a short ($\sim 10^{-6}$ nsec) time, these electrons return to their unexcited state, radiating photons of light. These photons are converted into photoelectrons at the cathode of a photomultiplier tube, causing a surge of electrons at the anode (see Figure 1).

The number of photons, and thus the surge of current, at the anode, is proportional to the total particle (kinetic) energy, E, unless the photomultiplier has reached its' saturation current. Figure 2 shows the graph of anode current vs. time. The area under the curve represents the total number of electrons, and therefore the total kinetic energy of the particle. In order to separate the signals of different particles from the photomultiplier pulse, two "gates" are used (Figure 3). These gates are timing signals generated to allow a portion of the photomultiplier pulse to be integrated. A fast gate integrates a signal with time constant $\tau_{\rm fast}$. A slow gate integrates the total pulse, proportional to E. A graph of fast signal vs. slow signal can yield a rough particle separation, as shown in Figure 4(a-d).

Finding E, however, does not determine the identity (2 and A) of the fragment, since a light particle with a large velocity may have the same kinetic energy as a heavy particle with a small velocity. An additional piece of information is required: dE/dx, the energy lost per unit length by the particle during its flight through the crystal. This involves attaching a thin slice of some scintillating material to the front of the thick crystal, and comparing the light outputs of the thin crystal and the thick crystal. The signal due to the thin crystal will be proportional to dE/dx, the amount of energy lost by the particle per unit length in the crystal. In addition, dE/dx also influences the shape of the photomultiplier pulse, which in turn can be used for particle

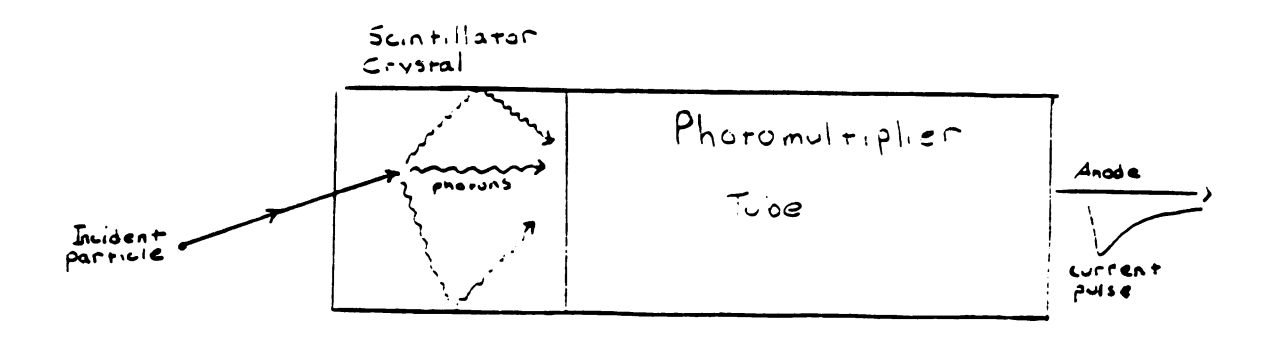


Fig. 1--Detector and Photomultiplier tube

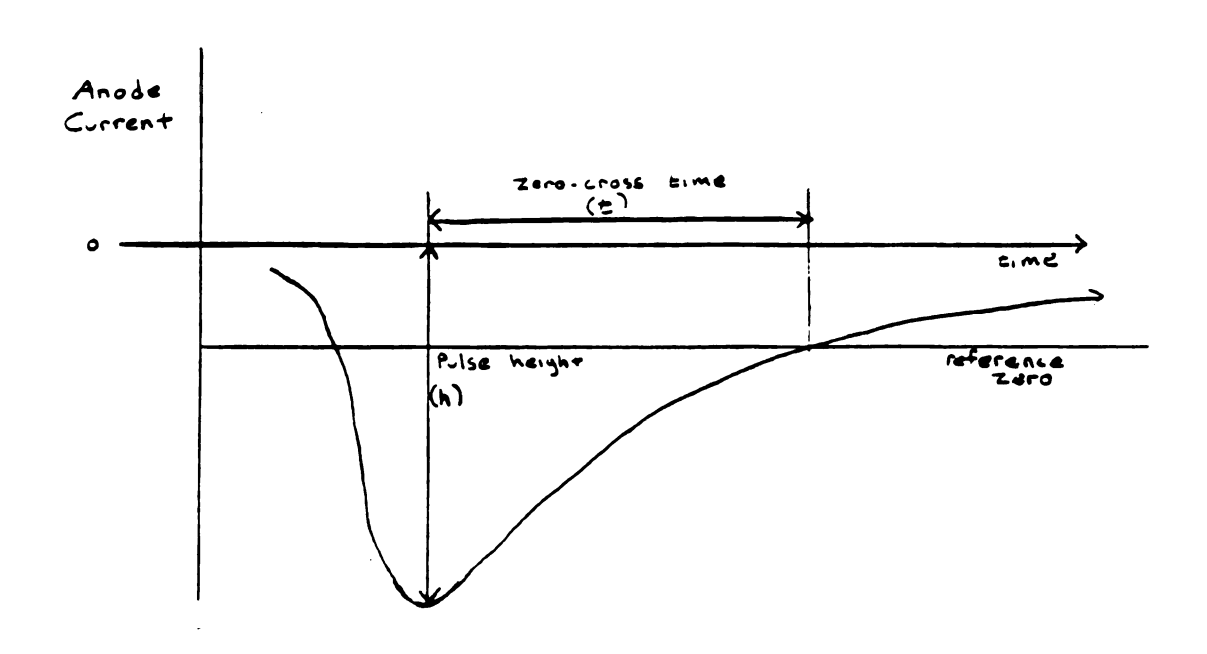


Fig. 2-- Photomultiplier Anode Current vs. Time

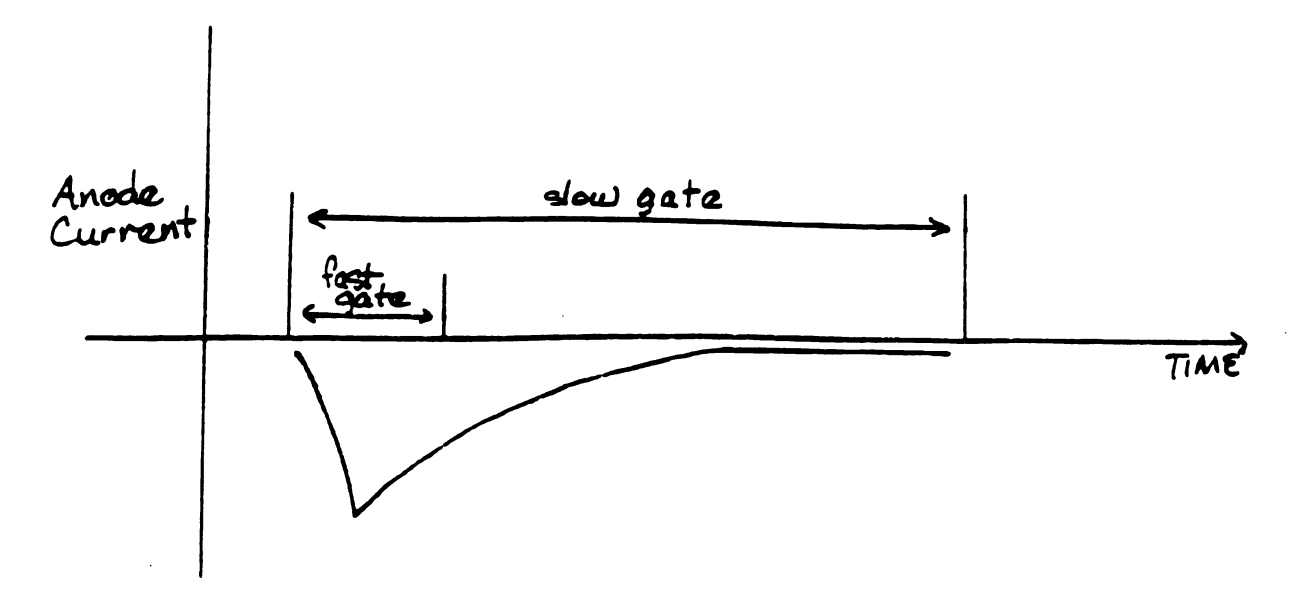


Fig. 3--Comparison of Fast and Slow Gates

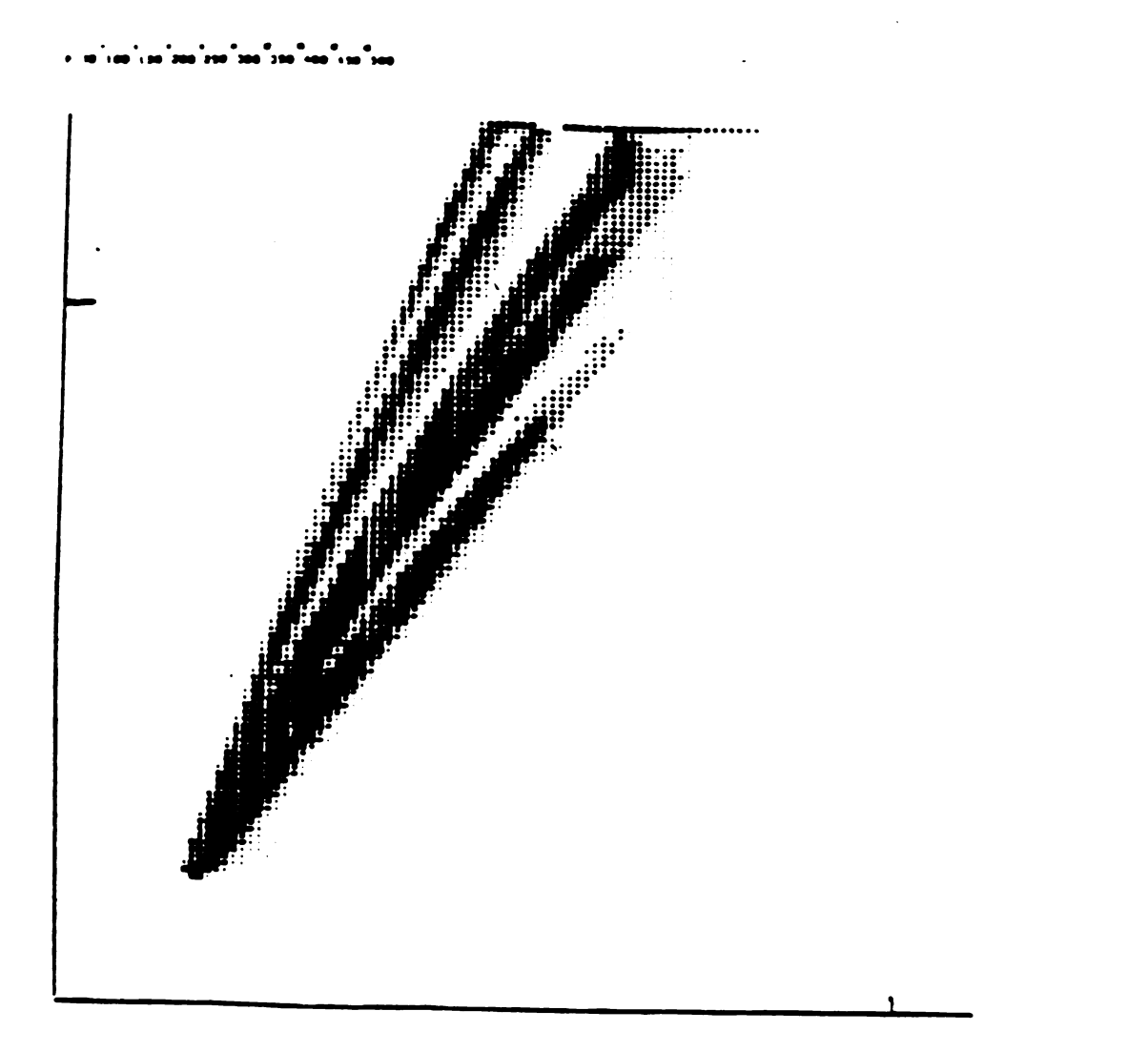


Fig. 4--(a) Fast Gate vs Slow Gate, CsI

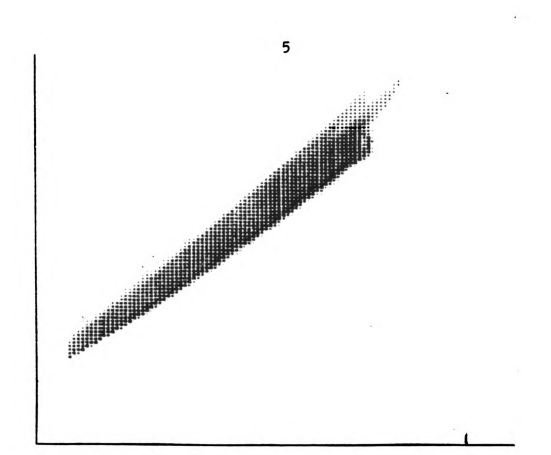


Fig. 4--(b) Fast Gate vs Slow Gate, BaF

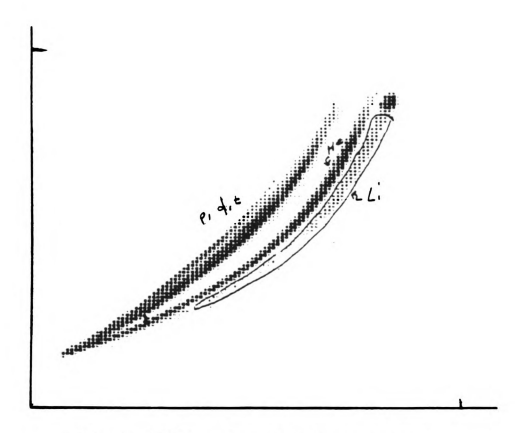


Fig. 4--(c) Fast Gate ys Slow Gate, NaI

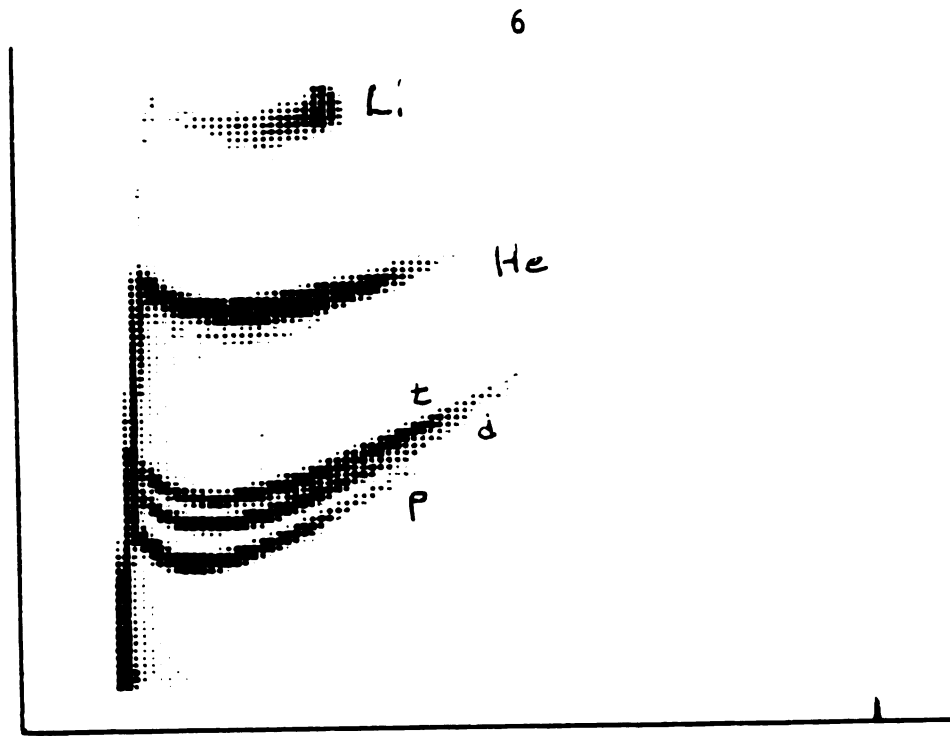


Fig. 4--(d) Fast Gate vs Slow Gate, Plastic

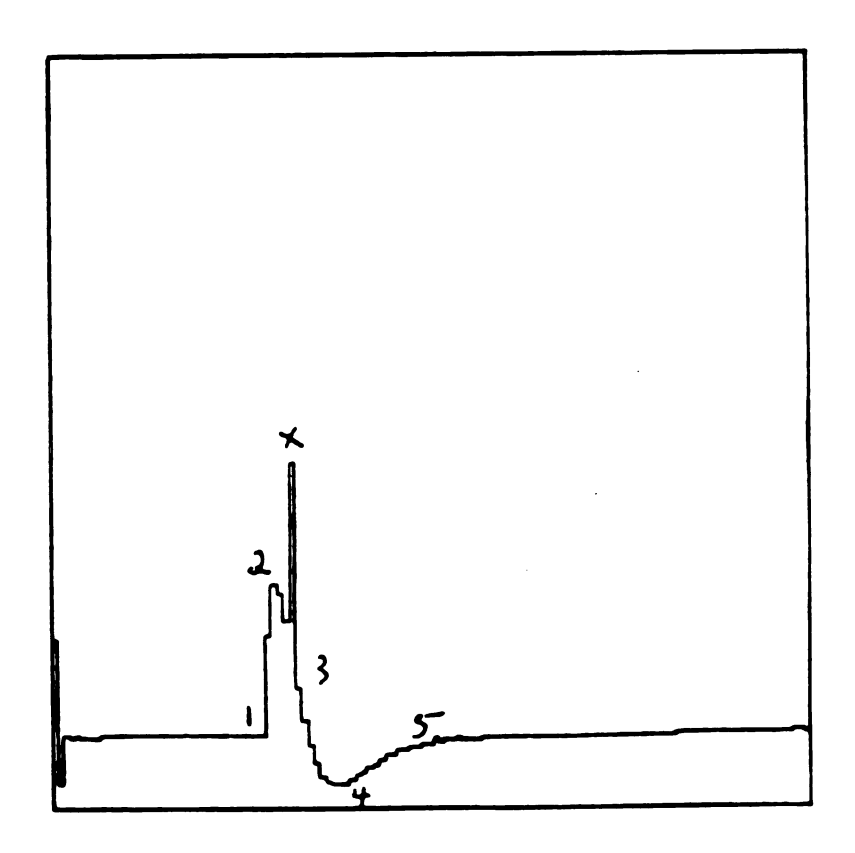


Fig. 5-- Digitization of Single Pulse, showing glitch and reference zero

discrimination. As Birke¹ explains, "The overall shape of the scintillation pulse depends on dE/dx, notably in CsI(Tl), so that this material can be used for pulse shape discrimination of different ionizing particles, in a manner similar to the organic scintillators." Thus, the relationship between dE/dx and E depends upon the particle type, as well as the energy.

A typical graph of dE/dx vs. E (Figure 9a) is demonstrated by a histogram of fast versus slow, with the points falling roughly into 'bands' of different isotopes after sufficient statistics have collected. In order to discriminate among isotopes, the experimenter must draw a contour around the band of interest on the finished graph. Here, a contour is drawn around the ³He band. The computer is then instructed to label all points within that contour as belonging to a certain isotope. The selected points can then be subjected to the experimenter's particular analysis. The main disadvantage of this method is that a single point on the graph conveys no information of particle type. Only after many points does the graph begin to show the band structure. Thus, a single data point can only be identified in relation to the rest of the data points. This requires the experimenter who is interested in particles of only one type to spend time recording particles of all types, which in turn lengthens the time necessary to complete an experiment. It is the aim of this project to develop a method to determine the identity of any single particle solely through analysis of a its dE/dx and E characteristics, thereby eliminating the need to record unnecessary data.

EXPERIMENTAL APPROACH

There are three methods of pulse discrimination discussed here. One involves digitizing the anode pulse with a flash encoder to find τ , the time constant of the pulse decay curve. This time constant is characteristic of the particle, but independent of the energy. The other two methods involve using the output of a zerocross filter to find the time, t, shown in Figure 2. An additional method, charge integration, involves collecting the charge from the pulse, which is proportional to the area under the curve in Figure 2. This area is also characteristic of the particle type. The zero-cross method was chosen instead of the charge integration method because it was less costly and presented fewer technical difficulties.

The first zero-cross method used to find τ was straightfoward: digitize the photomultiplier pulse as a function of time in 50 nsec bins, and find the time elapsed from the peak of the pulse to some arbitrary reference zero, as shown in Figure 2. The zero-cross time, t, is proportional to τ . Thus, knowing the time, t and the pulse height, h, τ can be found and calibrated to individual isotopes. A typical digitization is shown in Figure 5. A program was written to recognize the sequences labelled 1-5 in the data stream. If these five sequences occurred in order, the program recognized the data as a pulse, and recorded t and h. The program was also modified to smooth out a bit error in the flash encoder, marked X, which would occur randomly. These

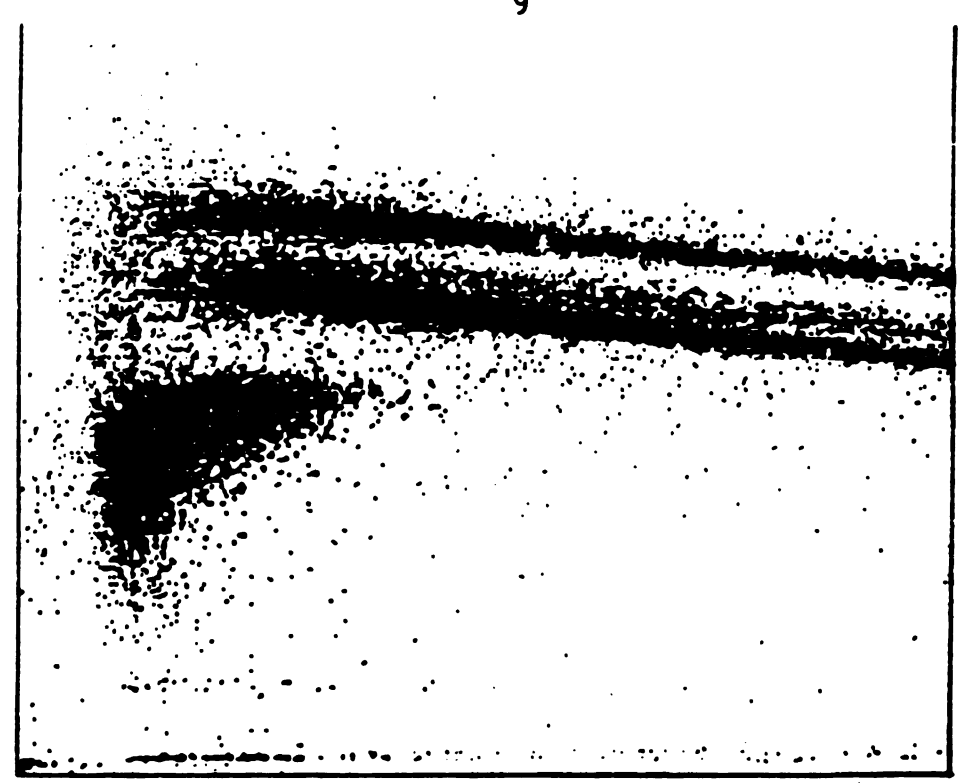


Fig. 6--(a) E (slow Gate) vs t

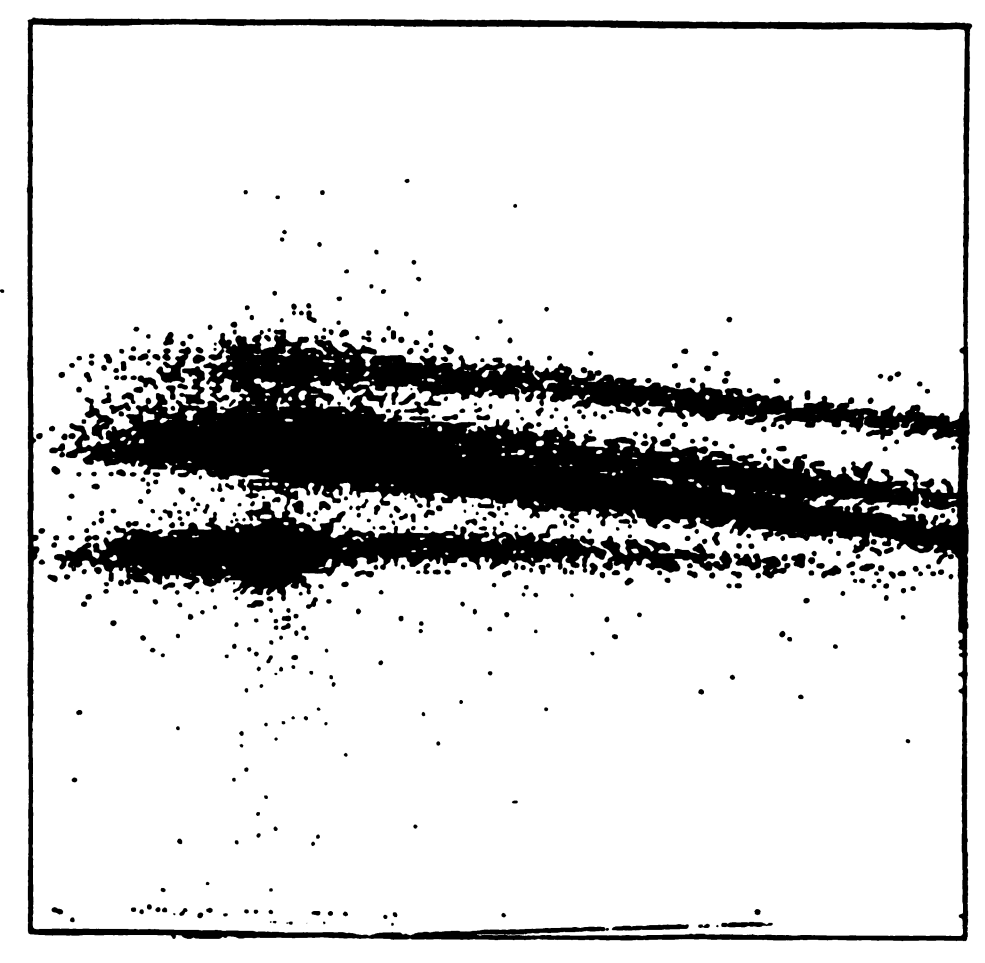


Fig. 6--(b) Fast Gate vs t

results, however, were inconsistent, yielding varying values of τ for alpha particles of different energies.

The second method of zero-cross-time particle discrimination consists of running the pulse through a filter which produces a bipolar pulse, and measuring the time from the leading edge to the crossover of the filtered pulse. This zero-cross time, t, was then plotted versus E. A graph of E vs. t (Figure 6a) should show the different types of particles as straight lines with zero slope. Instead, the lines showed a slope of -0.21, found empirically by replotting the histogram using a trial correction slope and comparing the resolutions of the Y-projection. Likewise, a graph of dE/dx vs. t (Figure 6b) showed a slope which varied for different isotopes.

With this method, the best resolution attained was barely enough to show the triton peak (Figure 7). The presence of this slope means that the relationship between E and t for a given τ is not constant, but depends on the total energy, E. The reason for this dependence is that the discriminator detects the centroid, or main surge, of charge from the photomultiplier tube. As E is increased, the fast component becomes larger and/or the slow component becomes smaller, moving the total charge centroid toward the beginning of the pulse. This leads to a difference in crossover time $(\Delta t_2 - \Delta t_1)$. This difference changes τ , making τ a function of energy as well as a function of particle type.

A third test of particle discrimination involved scattering a beam of lithium ions from a stationary target of gold atoms. The goal was to separate the different light fragments (protons, deuterons, tritons, He isotopes and Li isotopes) produced by the breakup of the Li ions during the collision. This method involved comparing dE/dx and E, using a silicon detector for the dE/dx signal. At present, particle

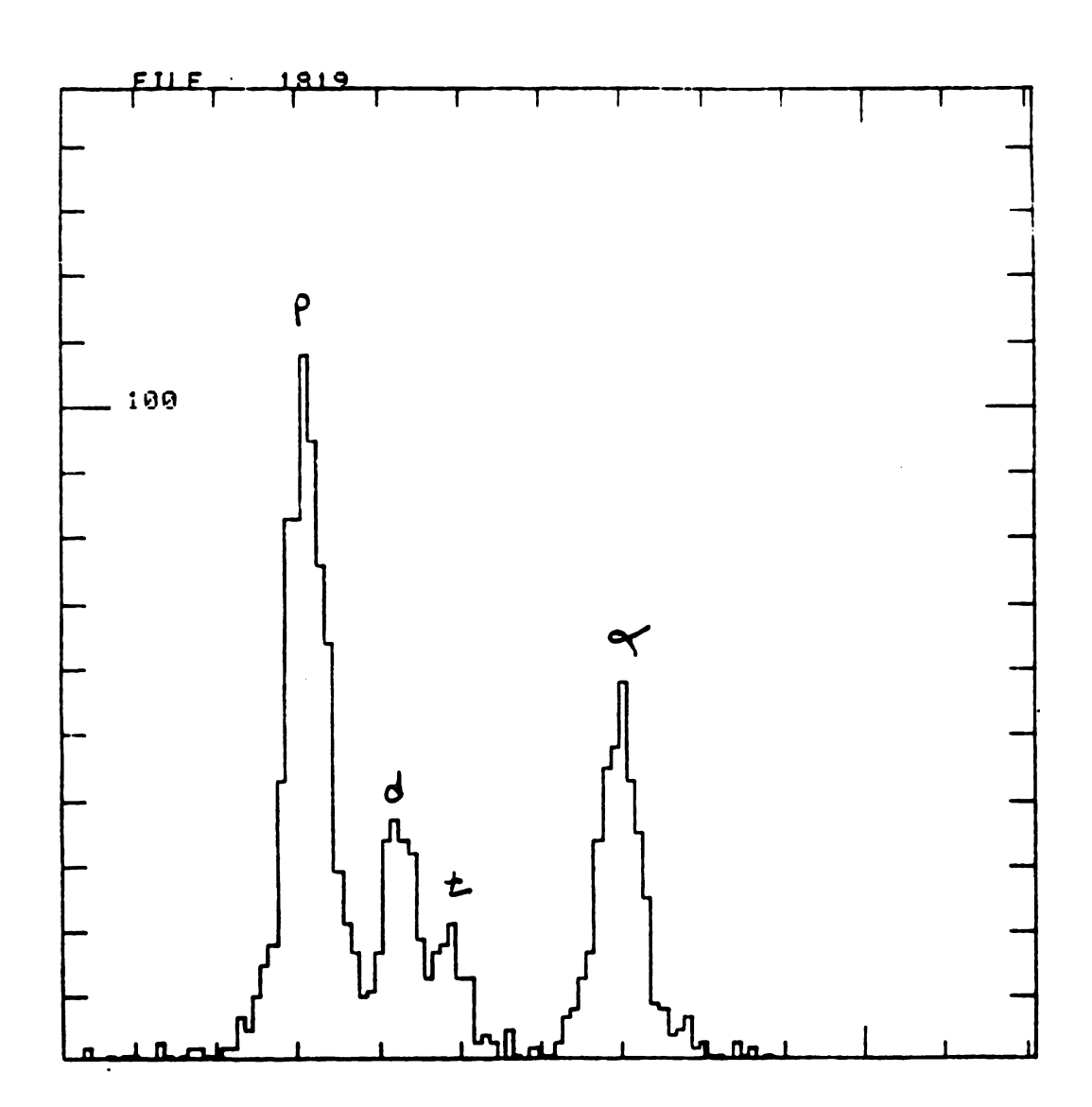


Fig. 7--Channel of Best Resolution, E vs t

discrimination can be performed by stacking many Si detectors together, to a thickness which allows E to also be found. However, Si detectors are costly, and another method was used. This consisted of using the Si for the dE/dx detector, and another standard scintillator for the E detector. We tried four different materials—BaF₂, CsI, NaI, and plastic (Fast BC412), and compared the resolution of the dE/dx vs. E graphs for each one. (Figure 9a-d) To further determine relative resolution, each of the graphs in Figure 9 was "sliced" at 5-channel intervals to find the maximum heights and separations between isotopes. This process was further refined to find the single channel of best resolution for each isotope. Typical channels of best resolution are shown for CsI in Figure 10a-d. On the basis of this, the CsI and BaF₂ results were chosen for further study.

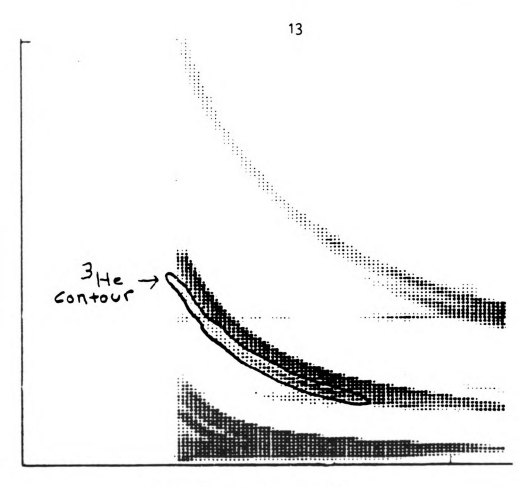


Fig. 9--(a) Si vs E, BaF2

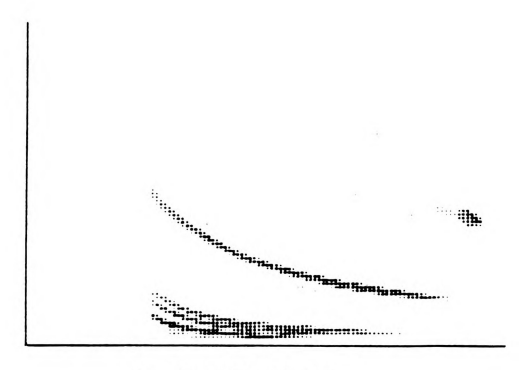


Fig. 9--(b) Si vs E, CsI

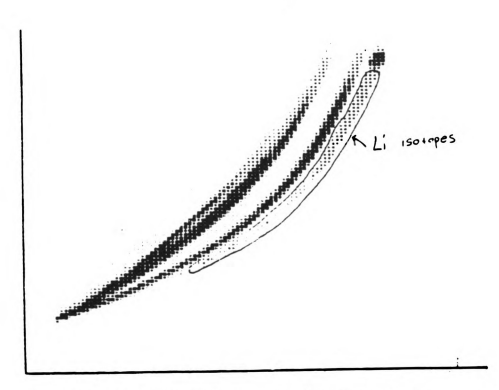


Fig. 9--(c) Si vs E, NaI, showing Li contour

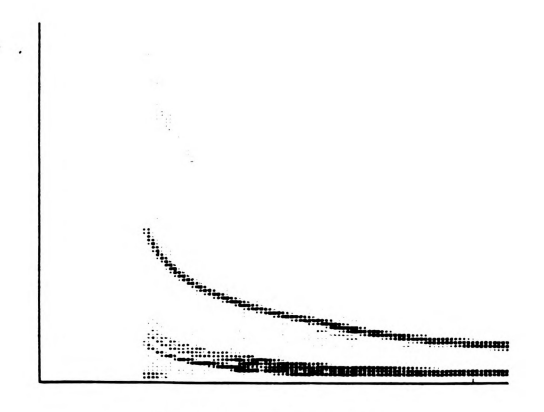


Fig. 9--(d) Si vs E, Plastic

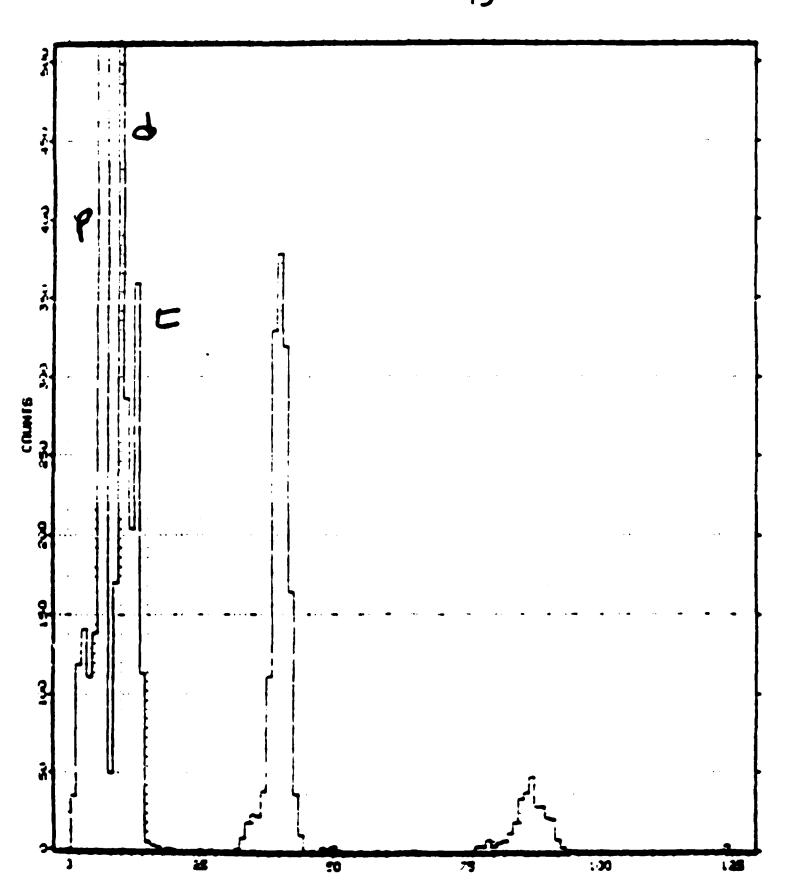


Fig. 10--(a) CsI Channel of Best Resolution; proton, deuteron, triton

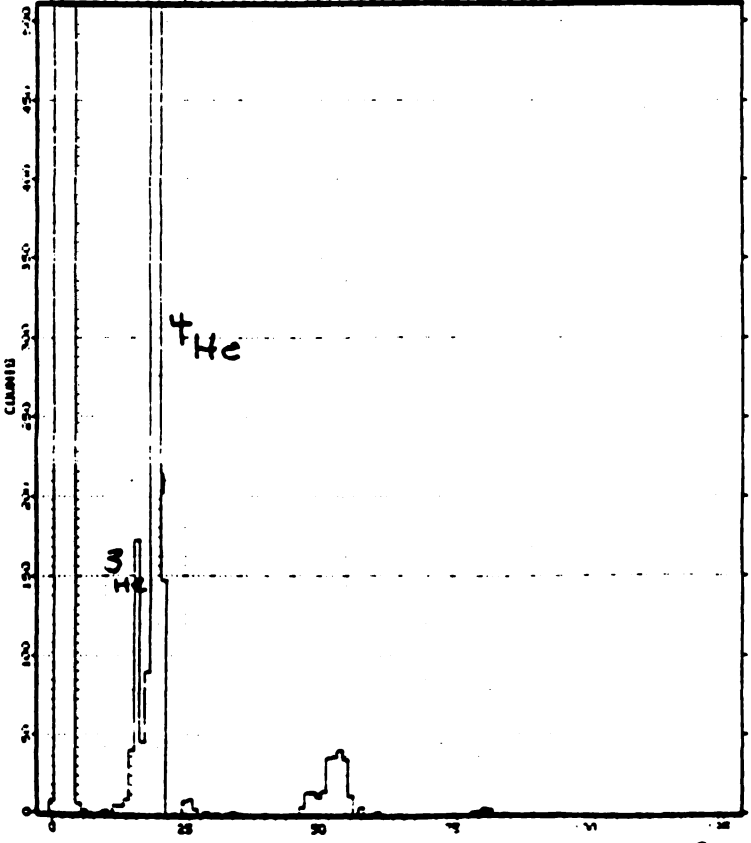


Fig. 10--(b) CsI Channel of Best Resolution; He³, He⁴

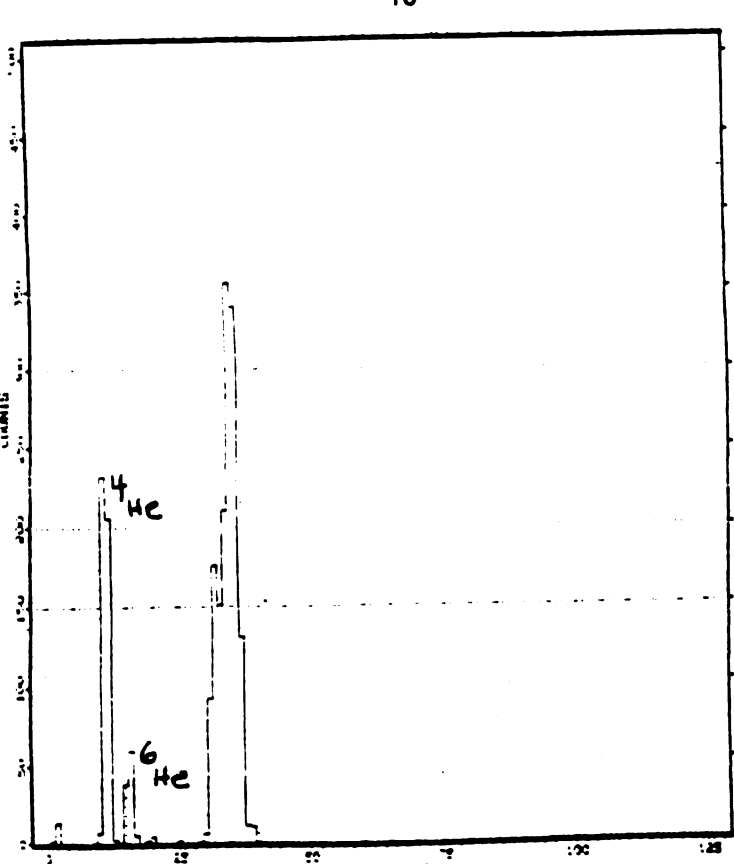


Fig. 10--(c) <u>CsI Channel of Best Resolution</u>; He⁴, He⁶

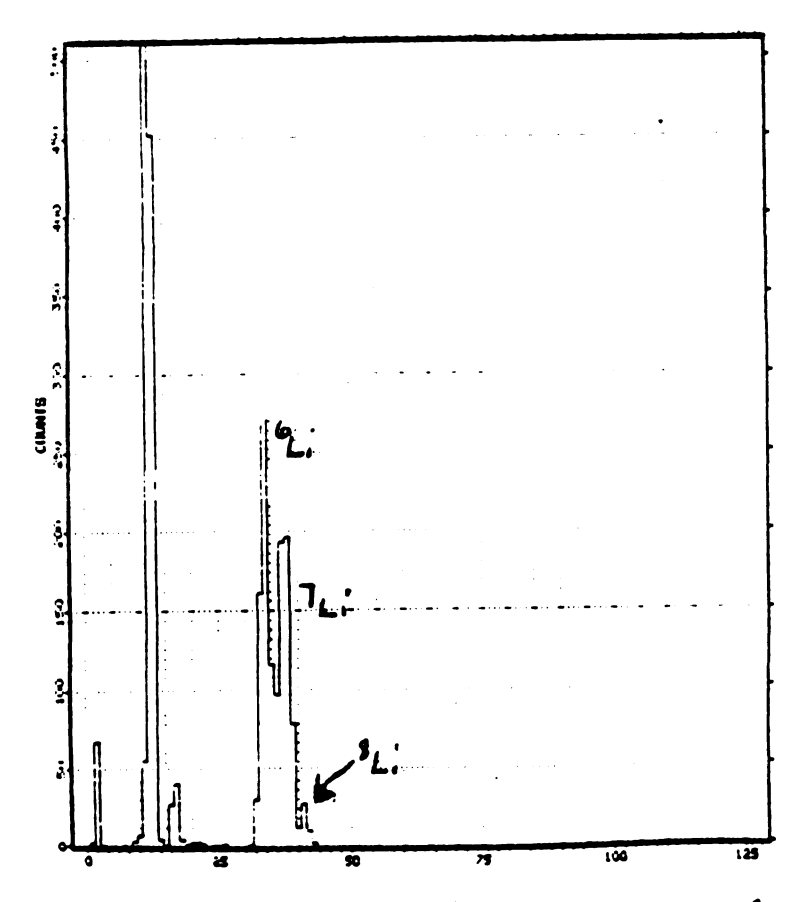


Fig. 10--(d) CsI Channel of Best Resolution; Li⁶, Li⁷

Since the relationship between the zerocross time and the total energy (Figure 6) depends on E, the next step was to calculate the expected total energy, $\mathbf{E}_{\mathrm{calc}}$, given only Z, A, and dE/dx, and find the relationship between zerocross time and E_{calc} . E_{calc} should be approximately equal to E, thus a graph of E_{calc} vs. E should be a straight line with slope=1. First, the data points of different isotopes must be separated from the dE/dx vs. E graph, using the contour method described earlier. The set of points for the ³He contour shown in Figure 9a is used as an example, and is shown in Figure 12(a). Since the determination of E_{calc} for a given value of Z, A, and dE/dx is quite time-consuming, only one point, the weighted average, from each channel was chosen. These points are shown in Figure 12(b). Since the value of dE/dx was also given as a channel number, it was necessary to first convert channel numbers into units of energy (Mev). This was done using a pulser calibrated in 10 Mev intervals, (Figure 11) and the value of Mev/channel was determined in the form y=mx+b, where m=0.2867 and b=-0.4233.

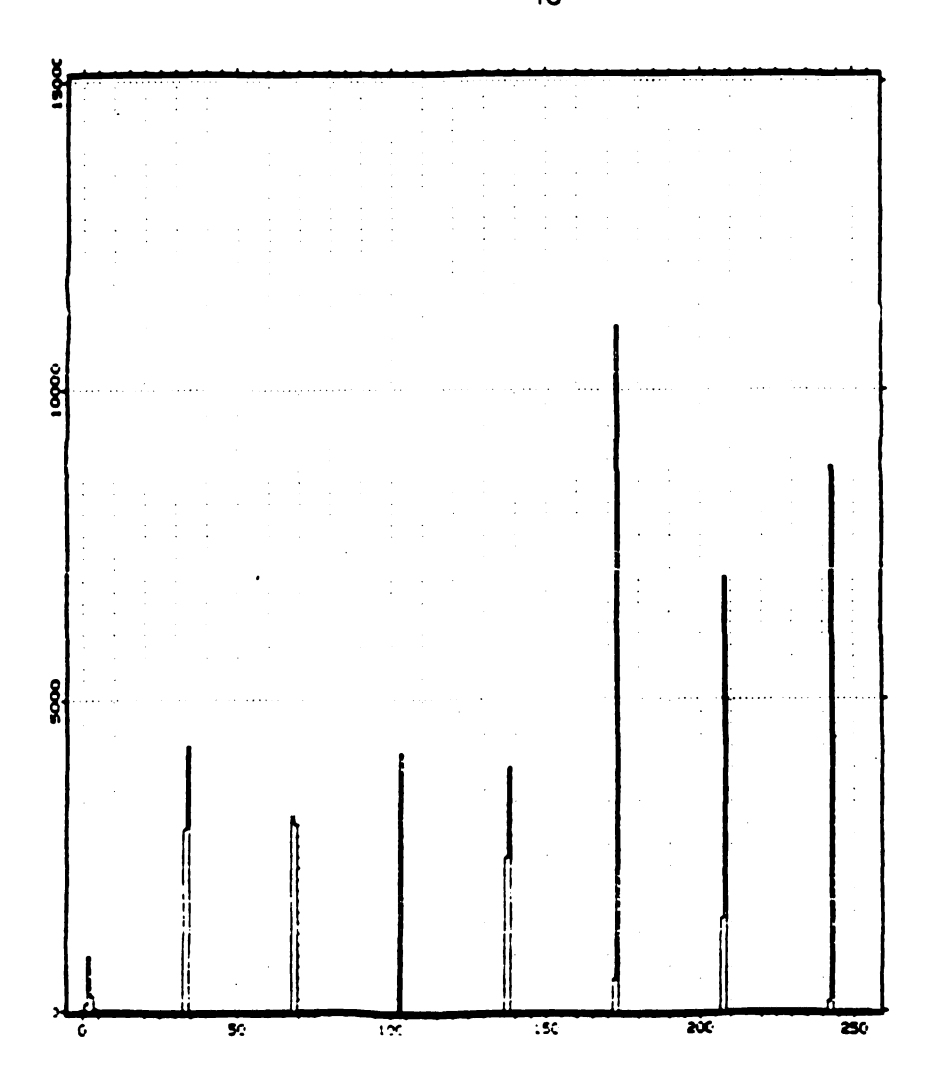


Fig. 11-- Pulser Calibration of Mev/Channel

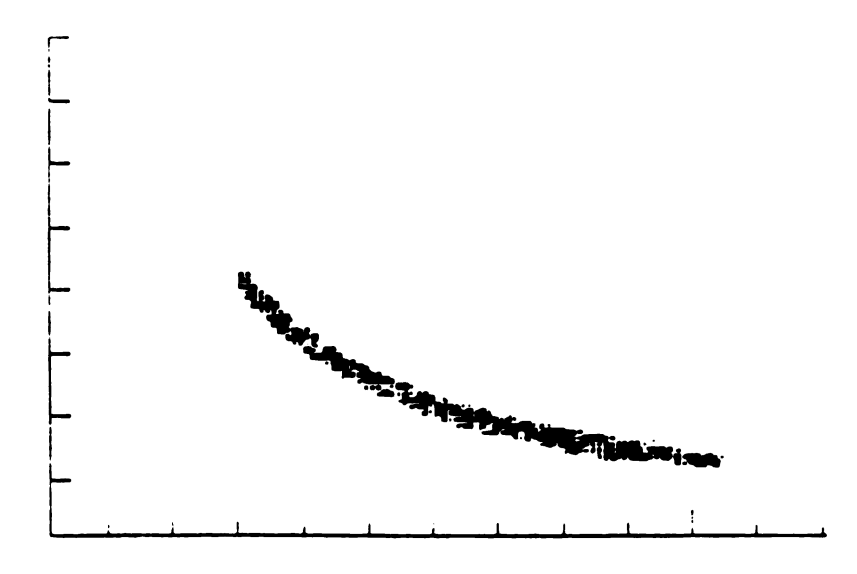


Fig. 12--(a) dE/dx (Si) vs E, CsI, ³He contour

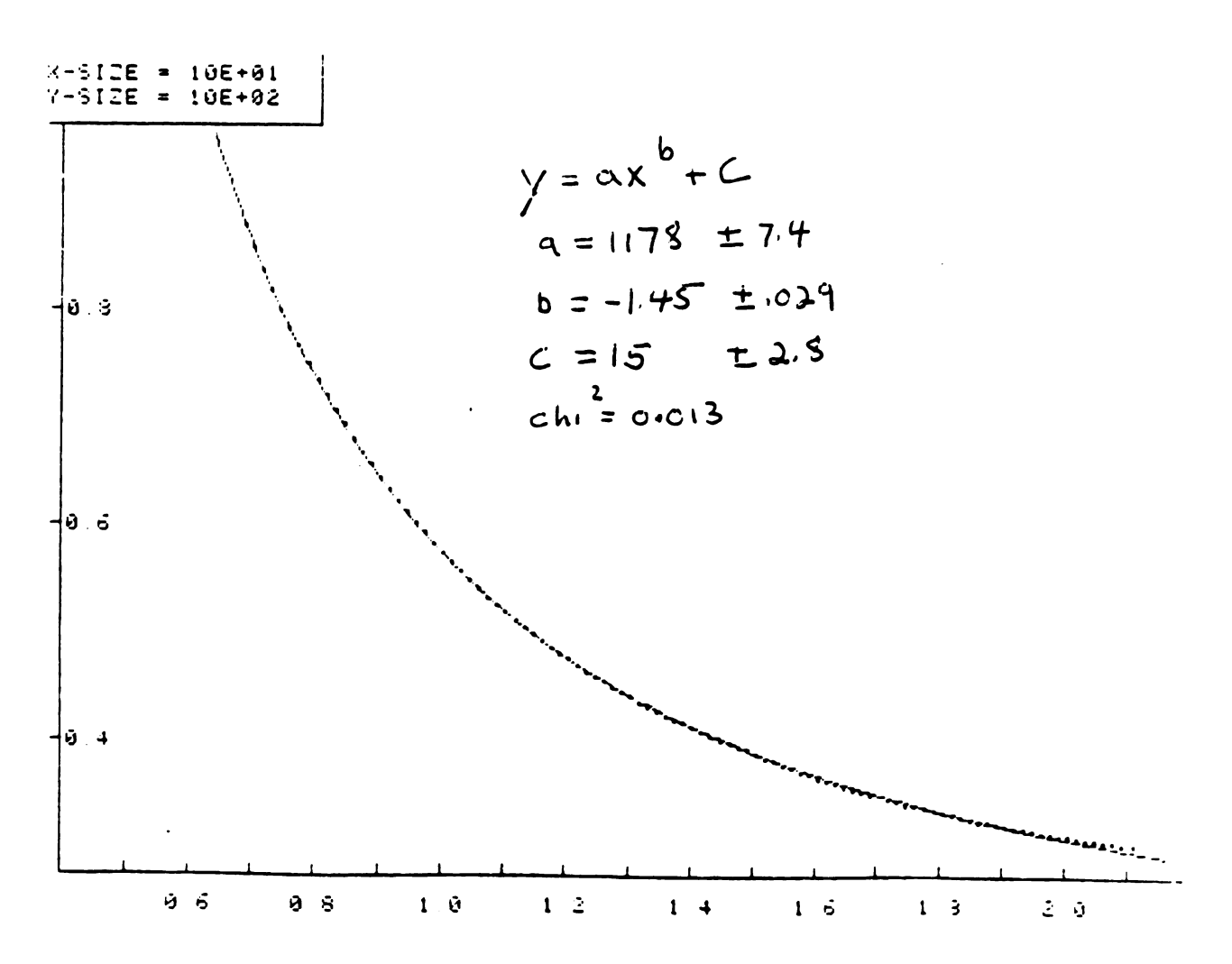


Fig. 12--(b) Power Law Fit for ³He Isotope

The next step was to determine $E_{\rm calc}({\rm dE/dx_{MeV}})$ for each point chosen. This was done by using a computer program designed to find therange (distance travelled in a Si detector) of a particle of given Z, A, and E. Using iterative techniques, this program could also be run in reverse to find E, if dE/dx, A, and Z are known. First, a trial energy $E_{\rm trial}$ is chosen (usually slightly greater than dE/dx), and the difference in ranges between RANGE($E_{\rm try}$) and RANGE($E_{\rm try}$ - dE/dx) is found. If this difference is slightly greater than or equal to the thickness of the Si detector, then $E_{\rm calc}=E_{\rm try}$. If not, then $E_{\rm try}=E_{\rm try}$ *1.01 and the program repeats. If there is no convergence after 1000 iterations, then the initial value of $E_{\rm try}$ must be changed. For Low Z, $E_{\rm try}=1.001$ * dE/dx, and ranges to $E_{\rm try}=2$ * dE/dx for high Z values, requiring trial-and-error adjustment for each isotope.

Next, the channel number and value of $E_{\rm calc}$ for each channel was run through the program LEASTSQR, which fit a power law of the form $Y=aX^b+c$ for each isotope. The fit of the 3 He contour from Figure 9a is shown in Figure 13. The values of a, b, and c for each isotope are then used to modify the SARA data-taking program. The modified SARA data-taking program is then run again, with all data points read from tape. This time, each value of dE/dx is put into the power law equation, which is much faster than the iterative method, and the values of $E_{\rm calc}$ are plotted against the E values for each point. However, the values of a, b, and c are correct only for points corresponding to a certain isotope. Thus, the data points for that isotope lie on one line with constant slope, while the points for all other isotopes lie on straight lines of varying slope. The constant slope is not equal to 1, however, since the energy absorption of the scintillator is different for different particles. The values of these constant slopes are then used to

calibrate the E values when the data-aquisition program is run again. Figures 13(a)-28(a) show the graphs of $E_{\rm calc}$ vs E for each isotope, for CsI and BaF₂. Figures 13(b)-28(b) show the channels of best resolution for each graph of $E_{\rm calc}$ vs E.

The last step was to run the data-aquisition program again, and graph $E_{\rm calc}$ vs Zerocross Time for the CsI scintillator, Figure 29(a). Since several values of $E_{\rm calc}$ exist for each point (one for each value of Z and A) and only one is correct, it is necessary to plot only those points where $E_{\rm calc}$ is approximately equal to E. In this way, the minimum difference ($E_{\rm calc}$ - E) can be set to optimize resolution. In Figs. 29(a) and 29(b), this difference was limited to 10 MeV. Figure 29(b) is a projection of Fig 29(a) onto the x-axis (time), resolving p,d,t as well as the He isotopes. As an added comparison, $E_{\rm calc}$ vs Fast Gate and $E_{\rm calc}$ vs Slow Gate are shown in Figs. 30(a) and 30(b), respectively.

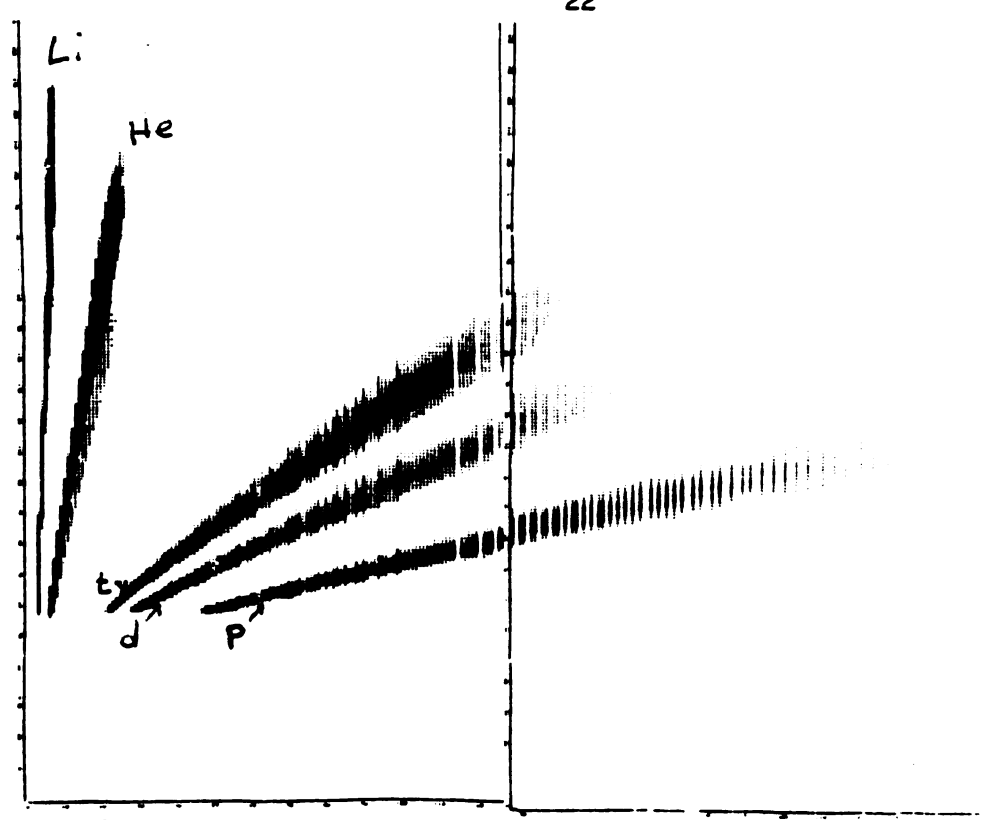


Fig. 13--(a) E_{cale} vs E, CsI, Calculated for Z=1, A=1

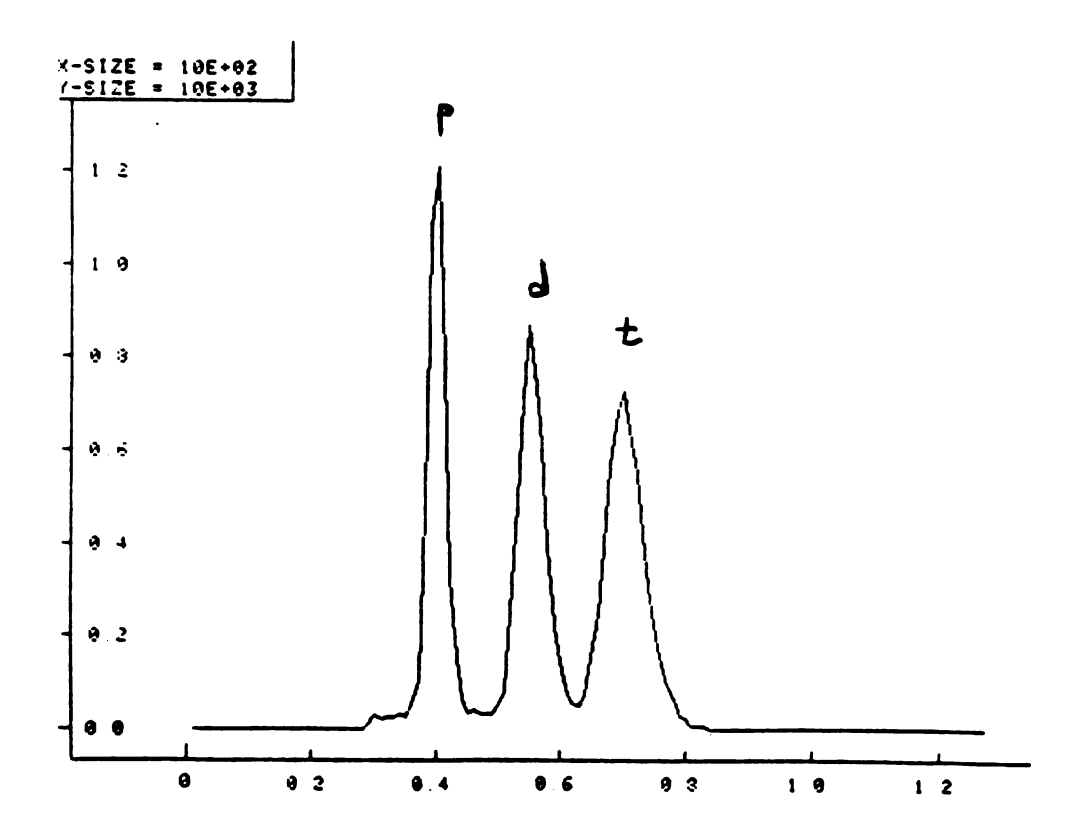


Fig 13--(b) Channel of Best Resolution, CsI, Z=1, A=1

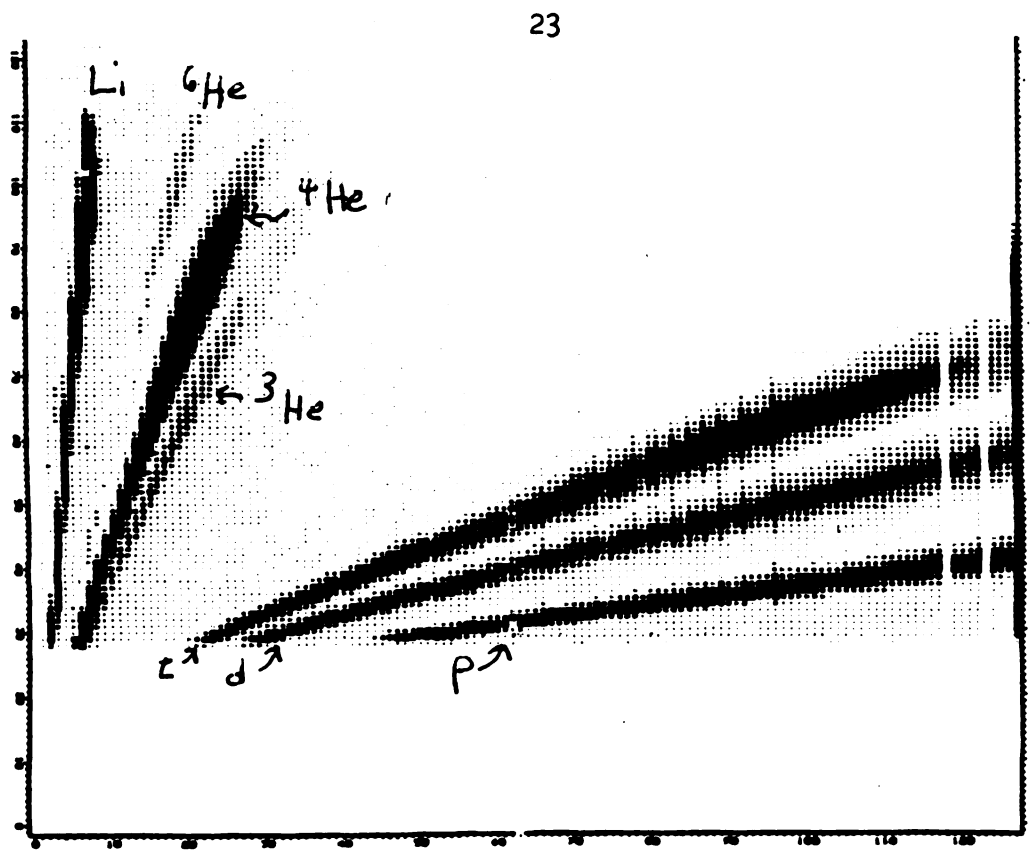


Fig. 14--(a) E_{calc} vs E, CsI, Calculated for Z=1, A=2

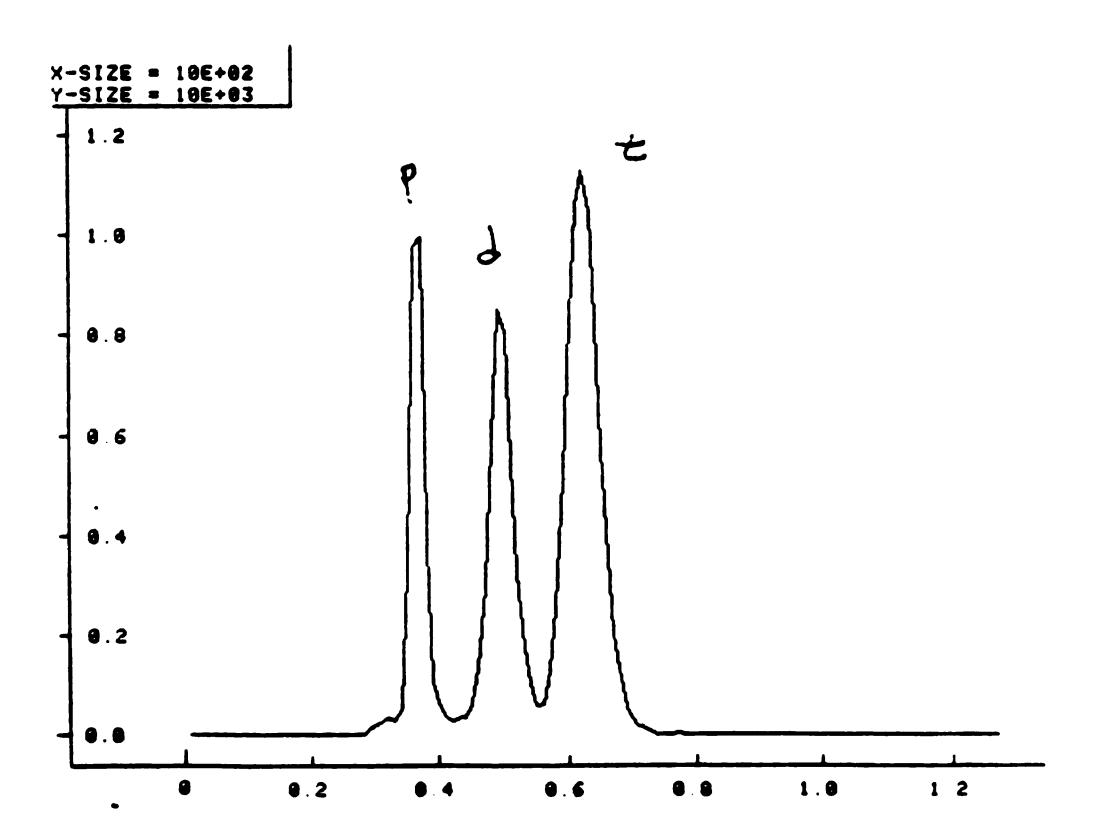


Fig 14--(b) Channel of Best Resolution, CsI, Z=1, A=2

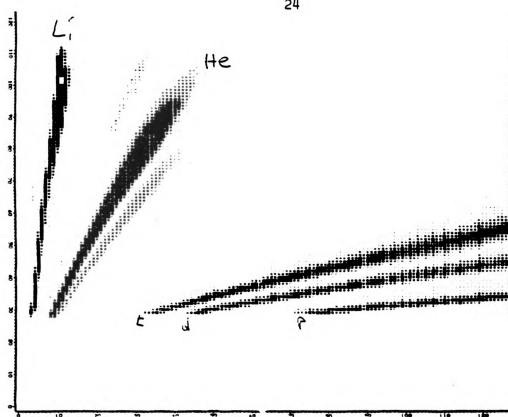


Fig. 15--(a) E_{calc} vs E, CsI, Calculated for Z=1, A=3

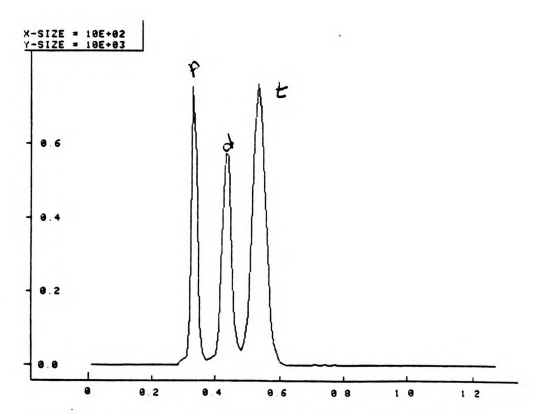


Fig 15--(b) Channel of Best Resolution, CsI, Z=1, A=3

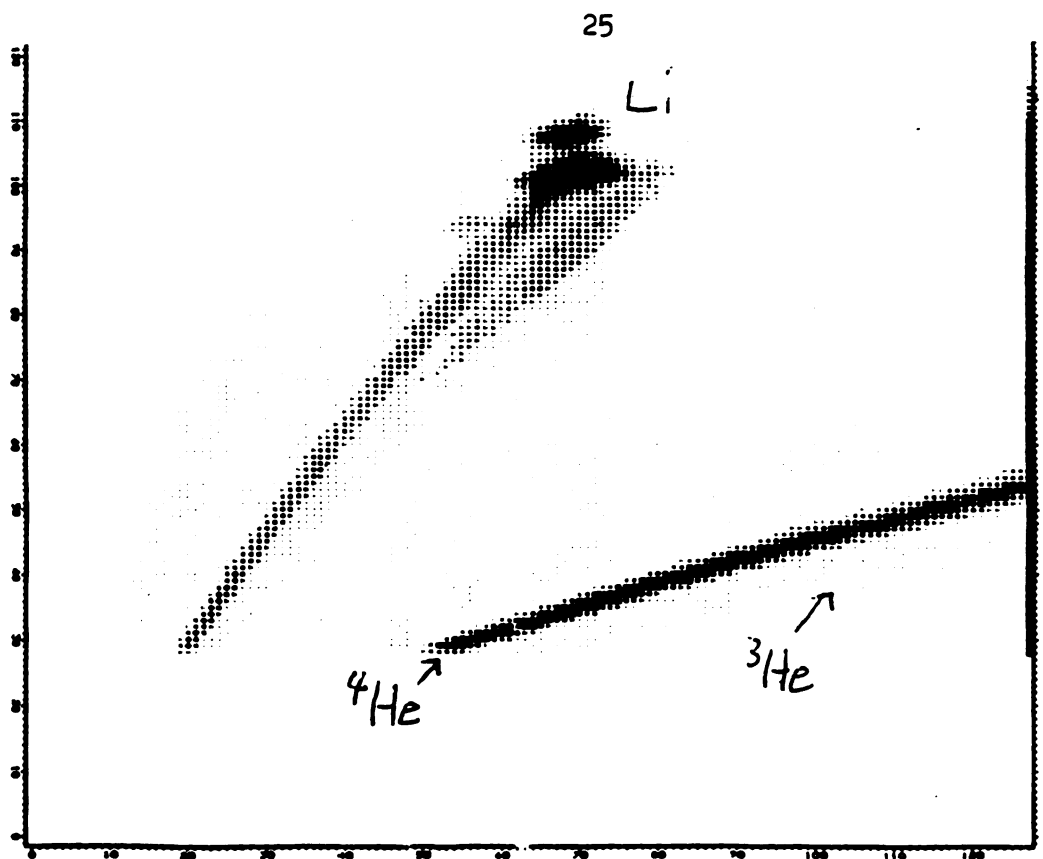


Fig. 16--(a) E_{calc} vs E, CsI, Calculated for Z=2, A=3

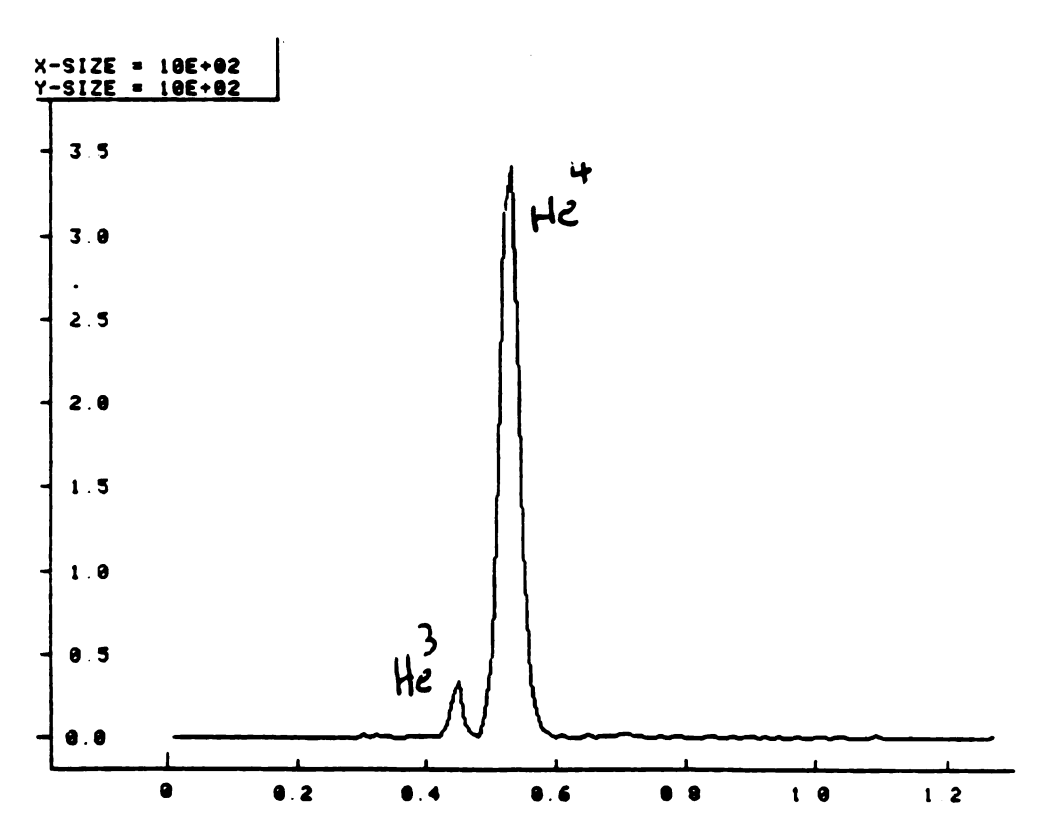


Fig 16--(b) Channel of Best Resolution, CsI, Z=2, A=3

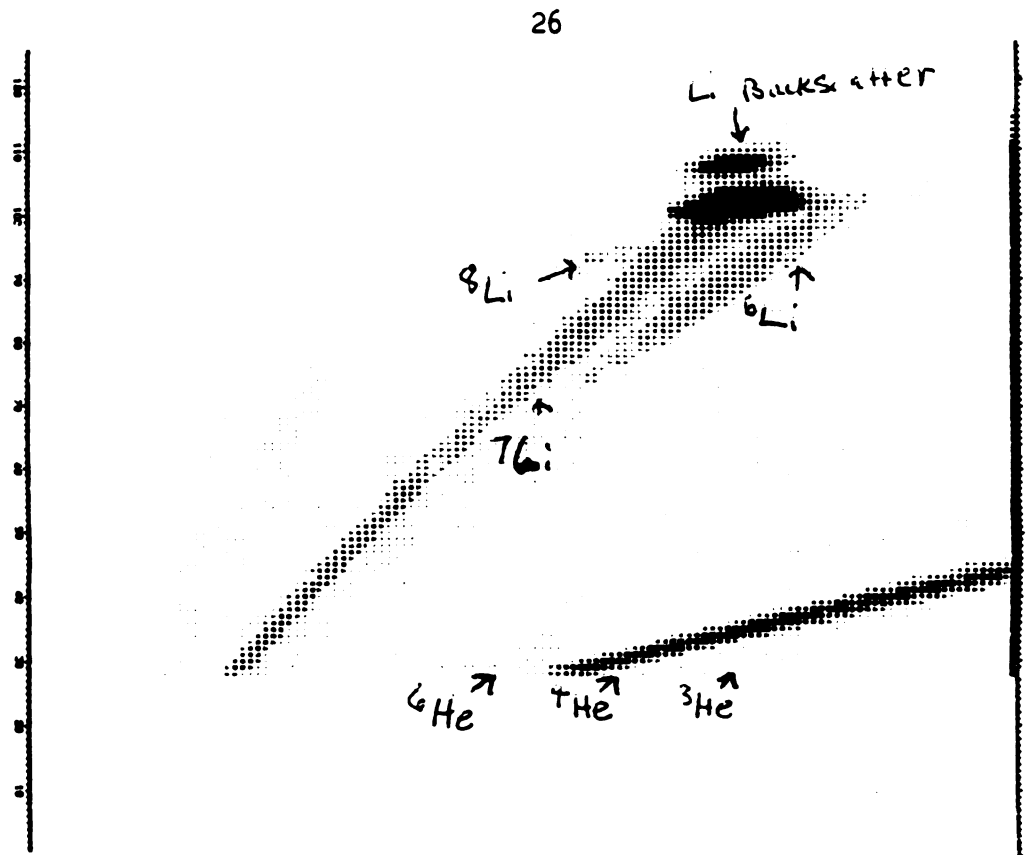


Fig. 17--(a) E_{calc} vs E, CsI, Calculated for Z=2, A=4

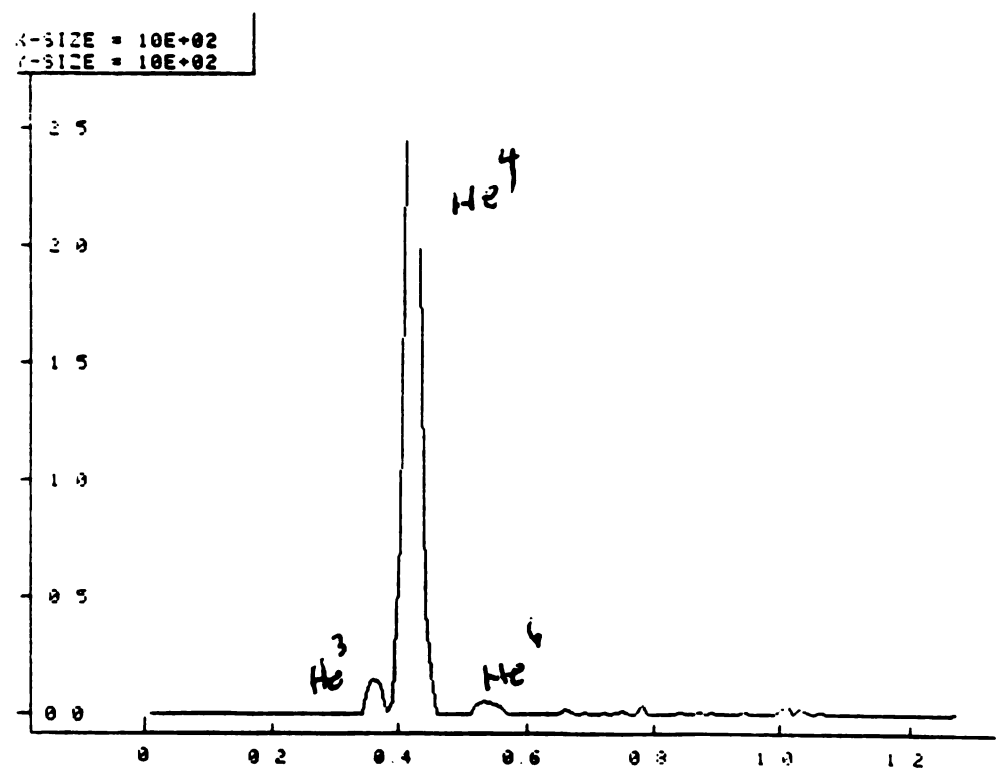


Fig 17--(b) Channel of Best Resolution, CsI, Z=2, A=4

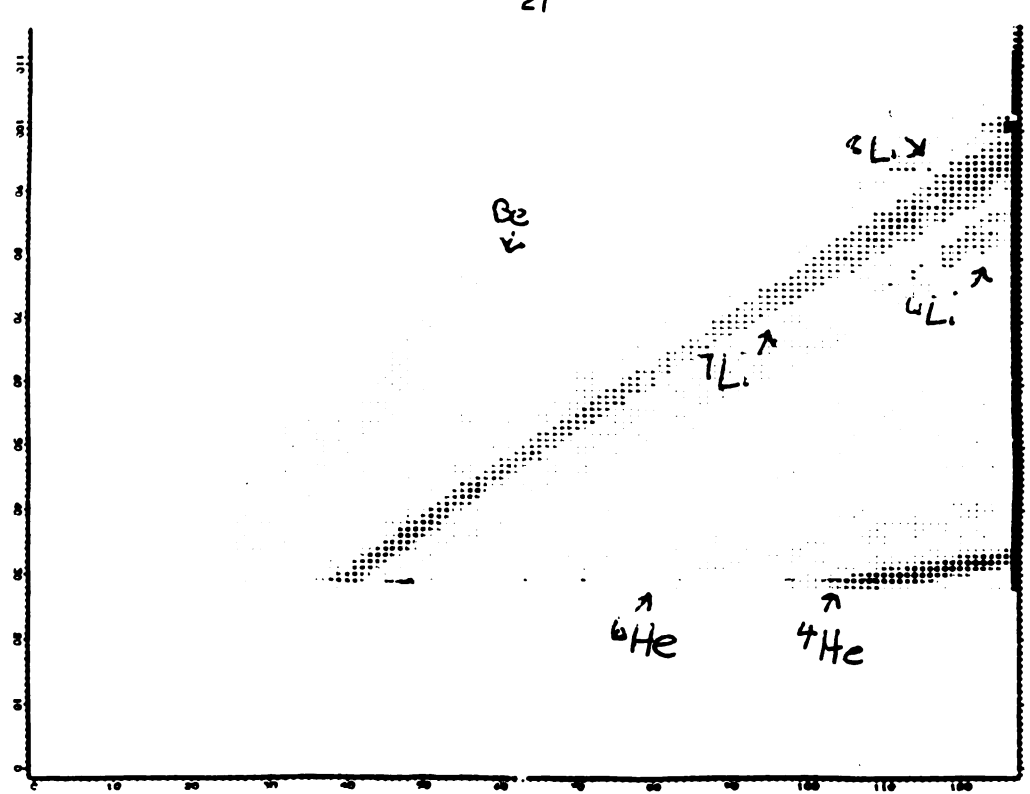


Fig. 18--(a) $\frac{E_{calc}}{calc}$ vs E, CsI, Calculated for Z=2, A=6

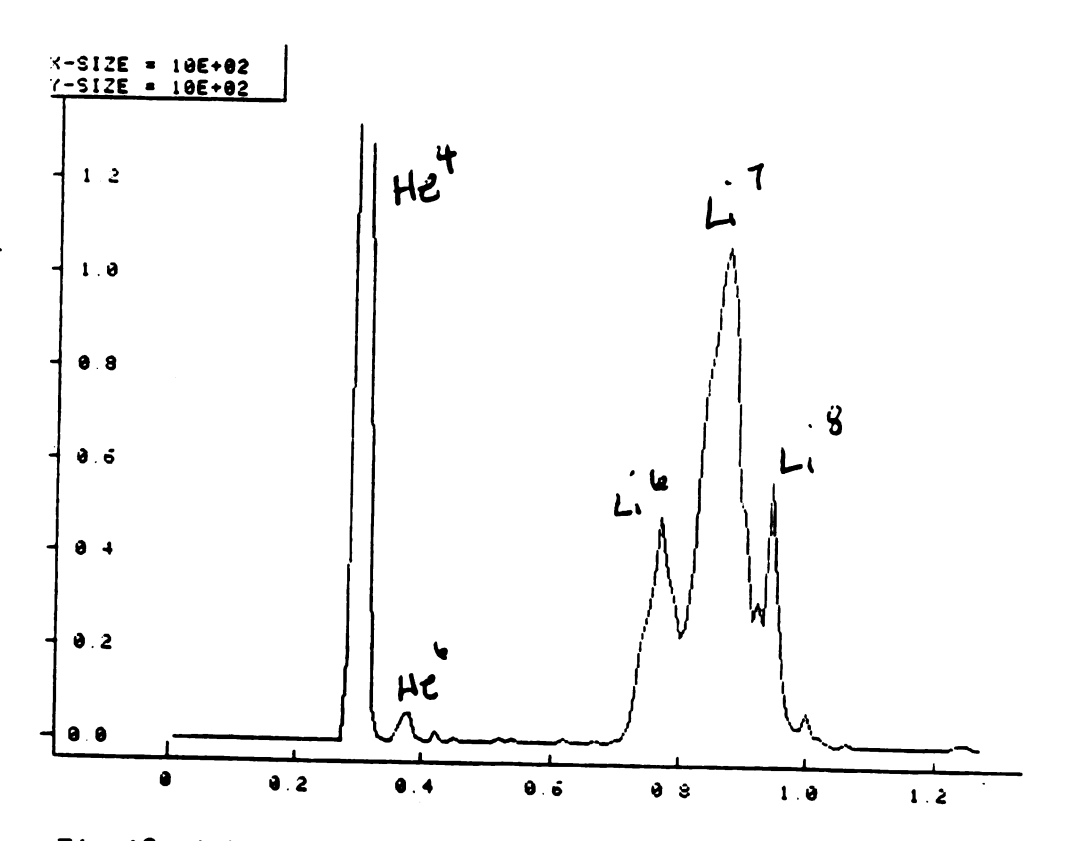


Fig 18--(b) Channel of Best Resolution, CsI, Z=2, A=6

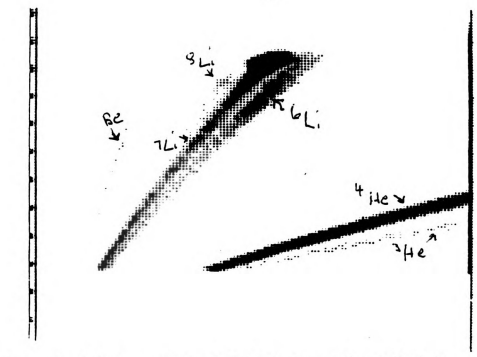


Fig. 19--(a) $\frac{E_{calc}}{E_{calc}}$ vs E, CsI, Calculated for Z=3, A=6

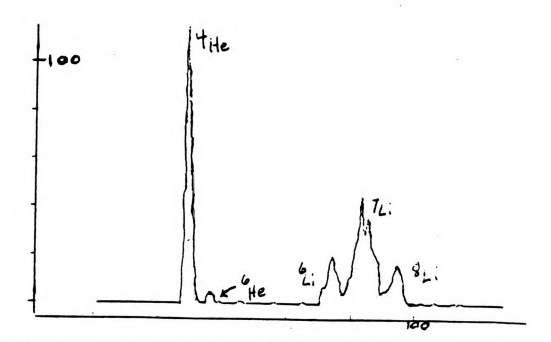


Fig 19--(b) Channel of Best Resolution, CsI, Z=3, A=6



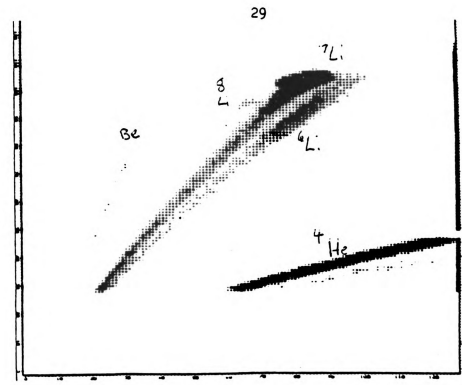


Fig. 20--(a) Ecale vs E, CsI, Calculated for Z=3, A=7

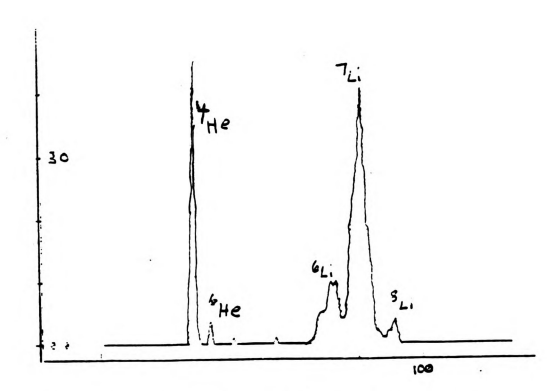


Fig 20--(b) Channel of Best Resolution, CsI, Z=3, A=7

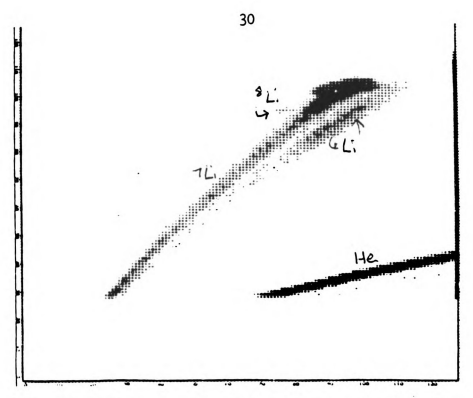


Fig. 21--(a) E_{calc} vs E, CsI, Calculated for Z=3, A=8

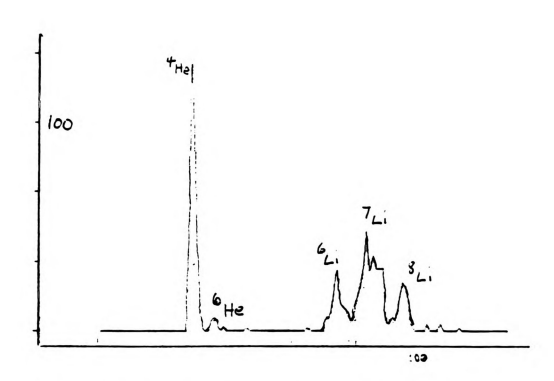


Fig 21--(b) Channel of Best Resolution, CsI, Z=3, A=8

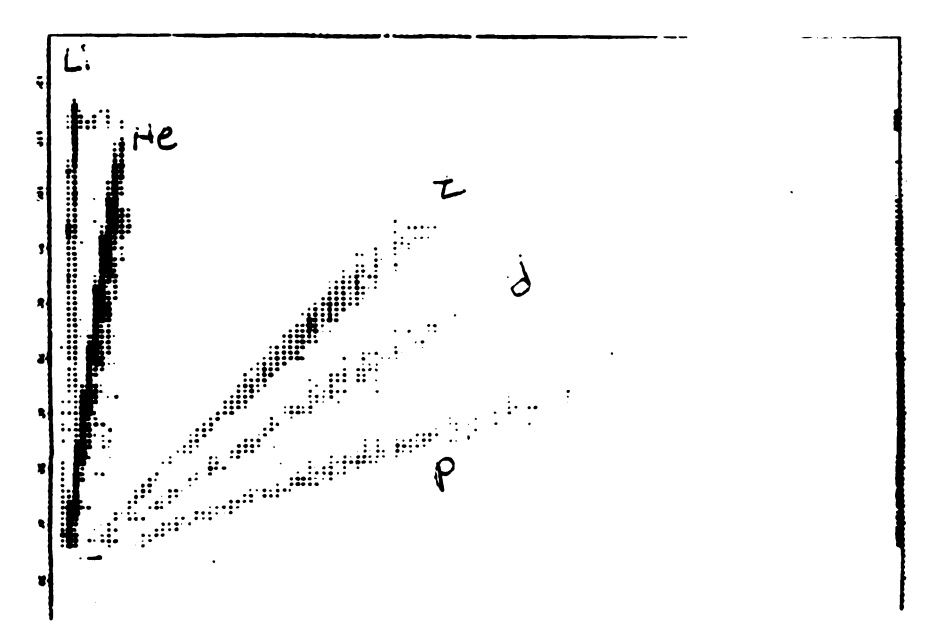


Fig. 22--(a) E_{calc} vs E, BaF₂, Calculated for Z=1, A=1

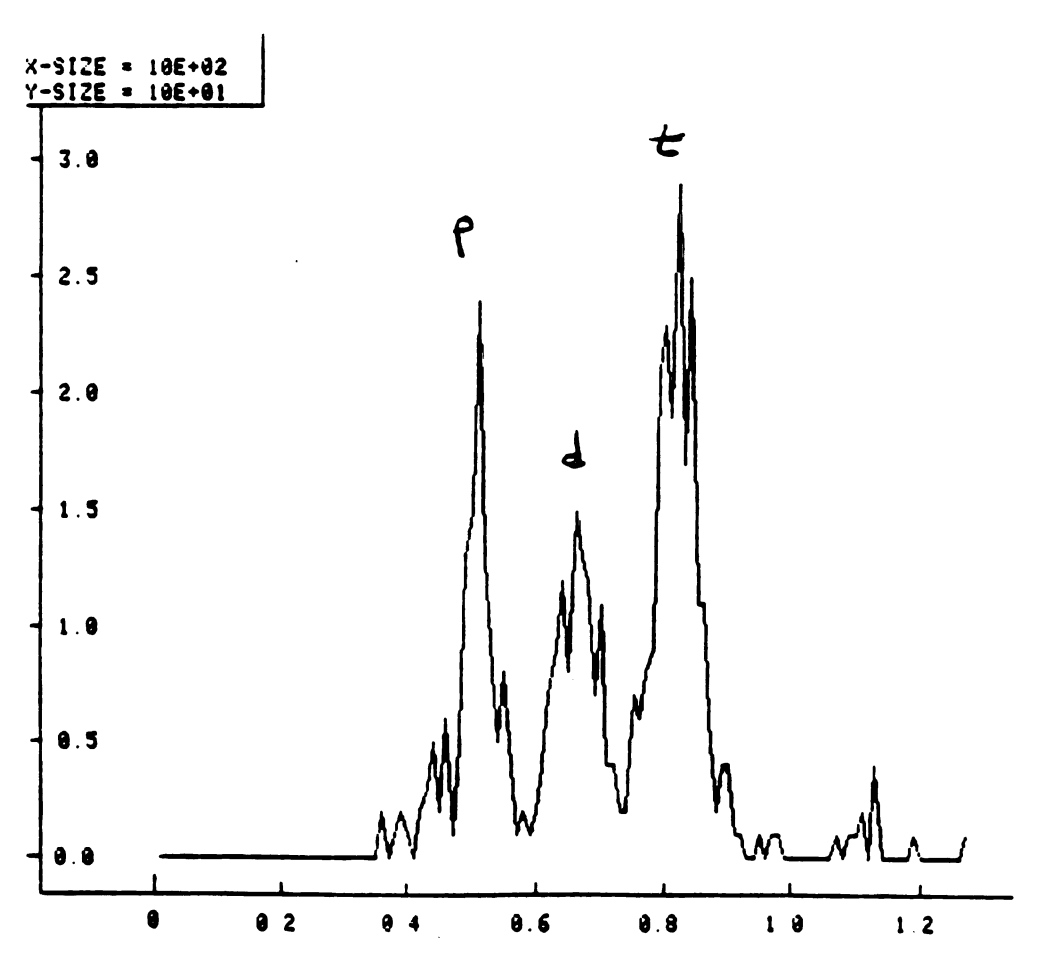


Fig 22--(b) Channel of Best Resolution, BaF₂, Z=1, A=1

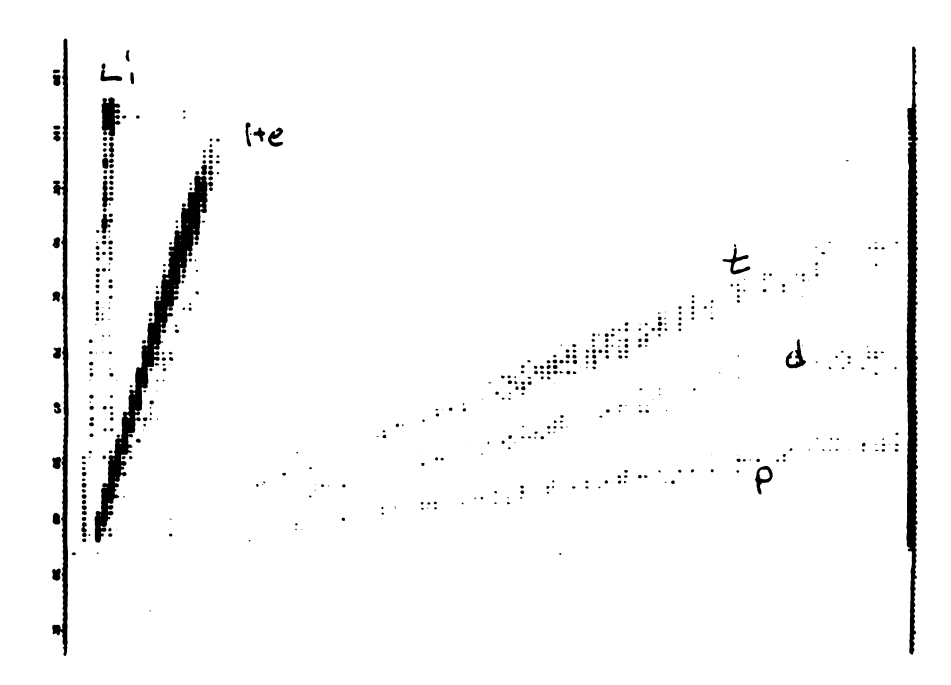


Fig. 23--(a) E_{calc} vs E, BaF_2 , Calculated for Z=1, A=2

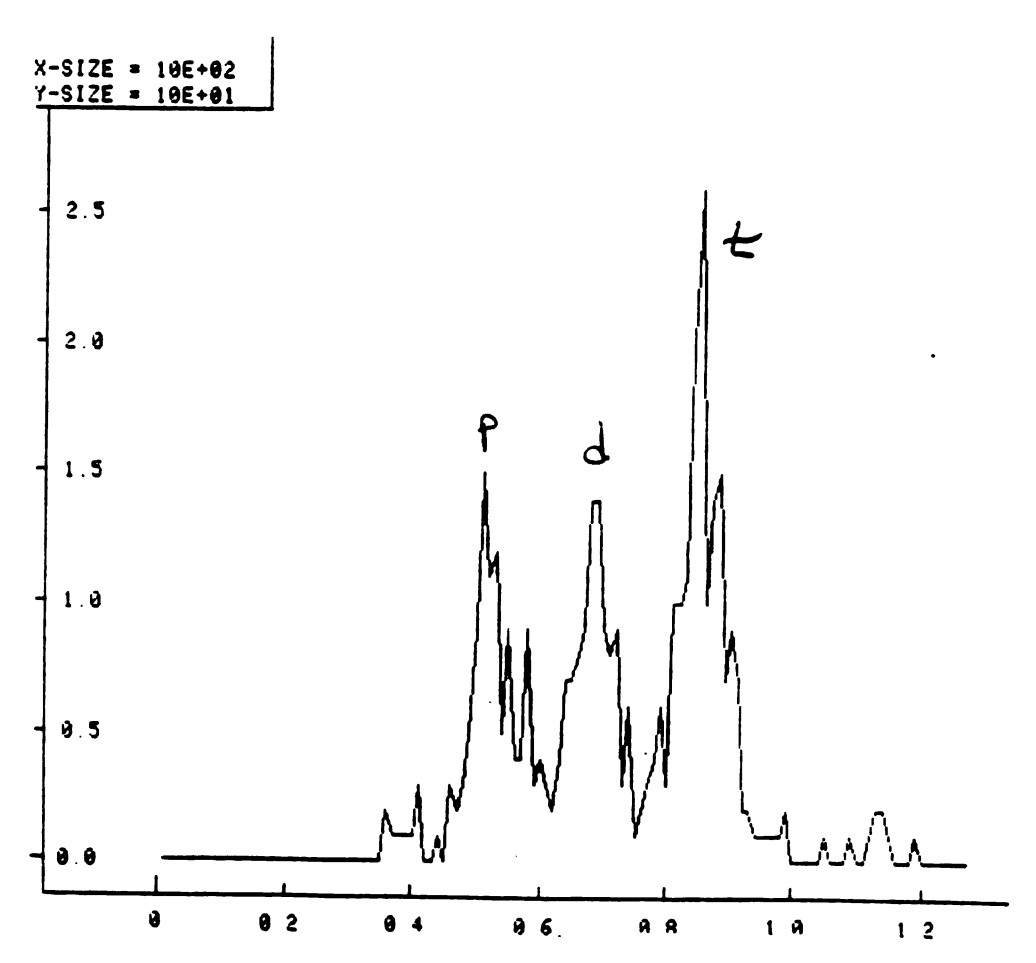


Fig 23--(b) Channel of Best Resolution, BaF₂, Z=1, A=2

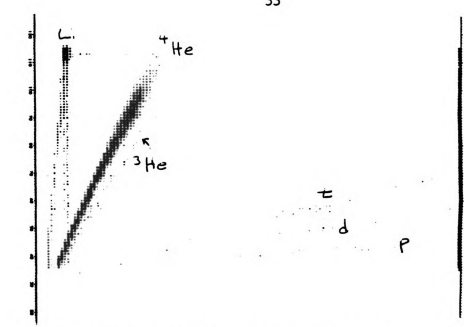


Fig. 24--(a) E_{calc} vs E, BaF_2 , Calculated for Z=1, A=3

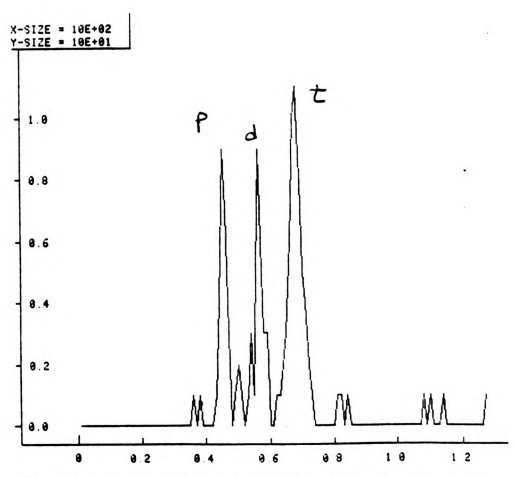


Fig 24--(b) Channel of Best Resolution, BaF2, Z=1, A=3

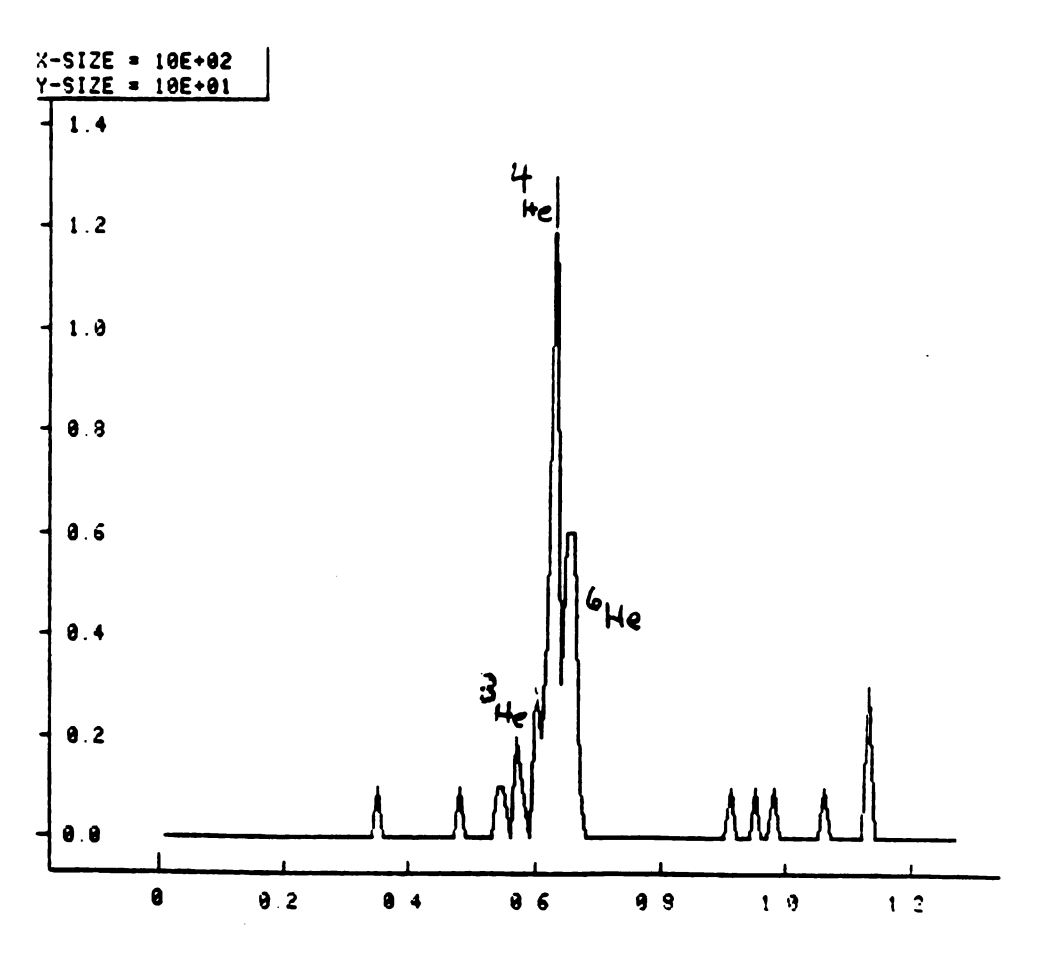


Fig 25--(b) Channel of Best Resolution, BaF₂, Z=2, A=3

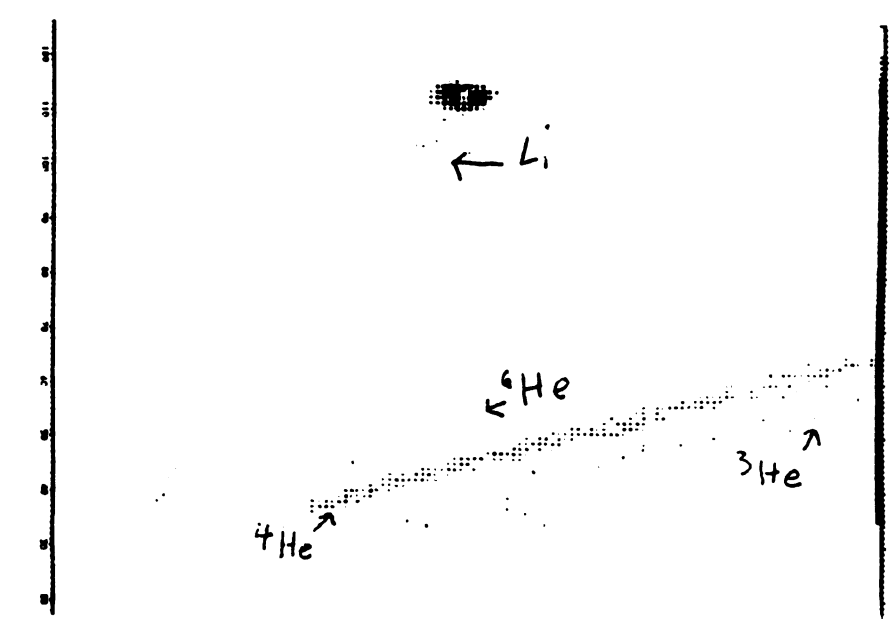


Fig. 25--(a) E_{calc} vs E, BaF₂, Calculated for Z=2, A=3

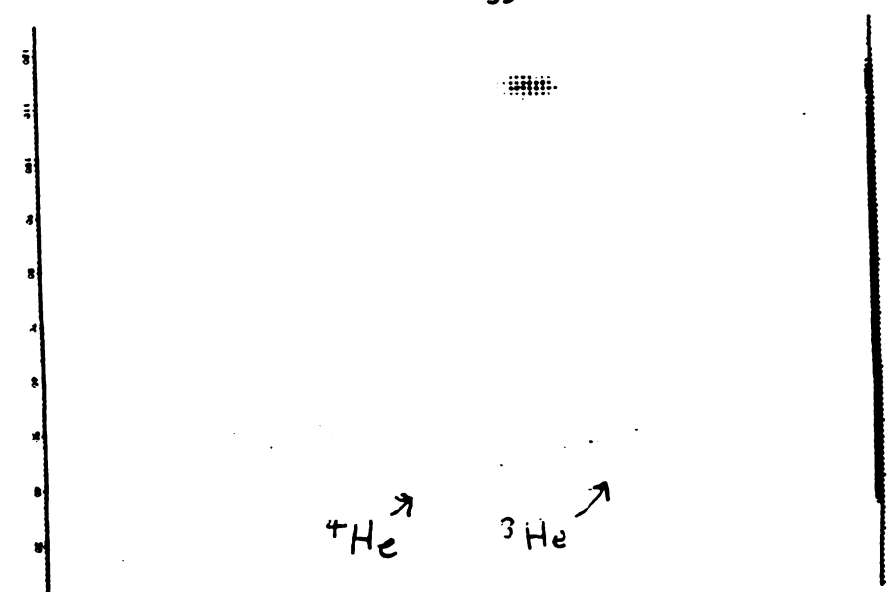
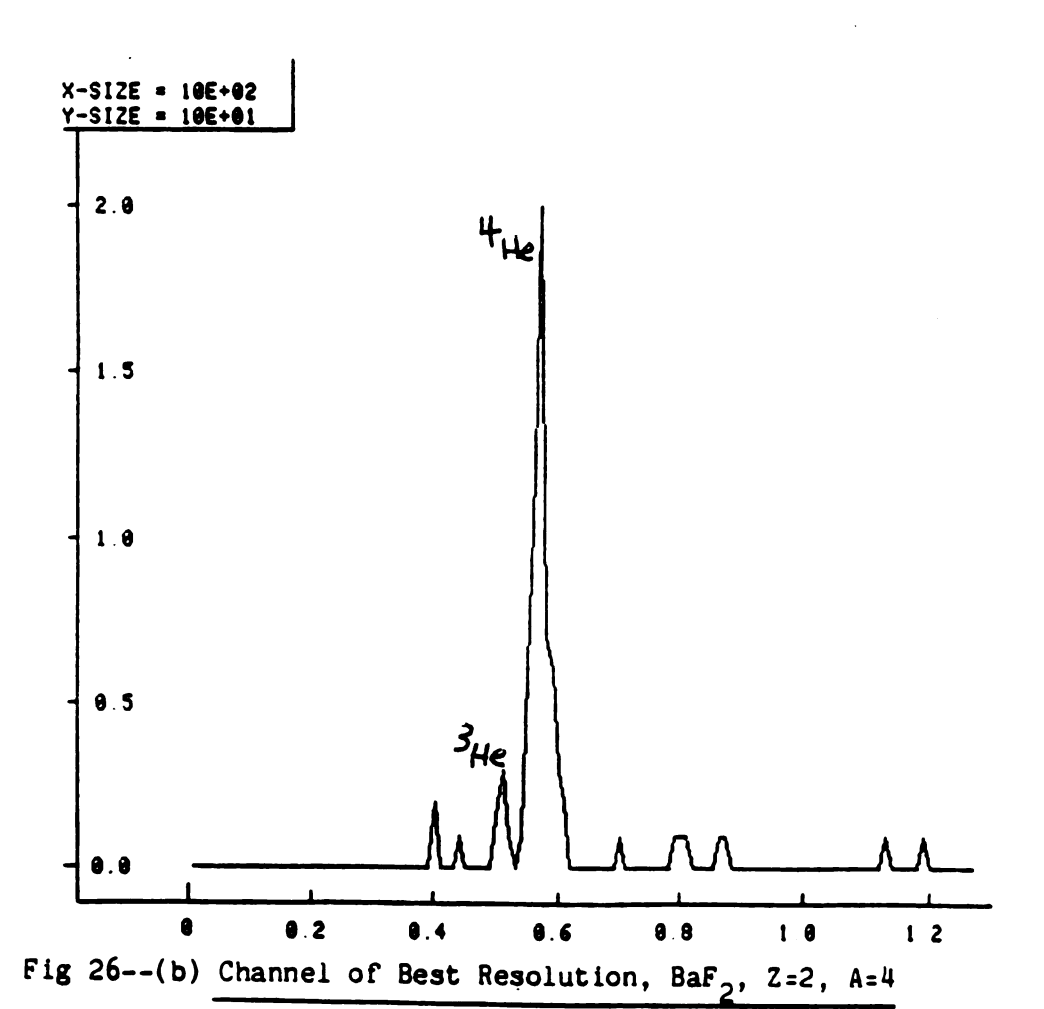


Fig. 26--(a) $\frac{E_{calc}}{calc}$ vs E. BaF₂, Calculated for Z=2, A=4



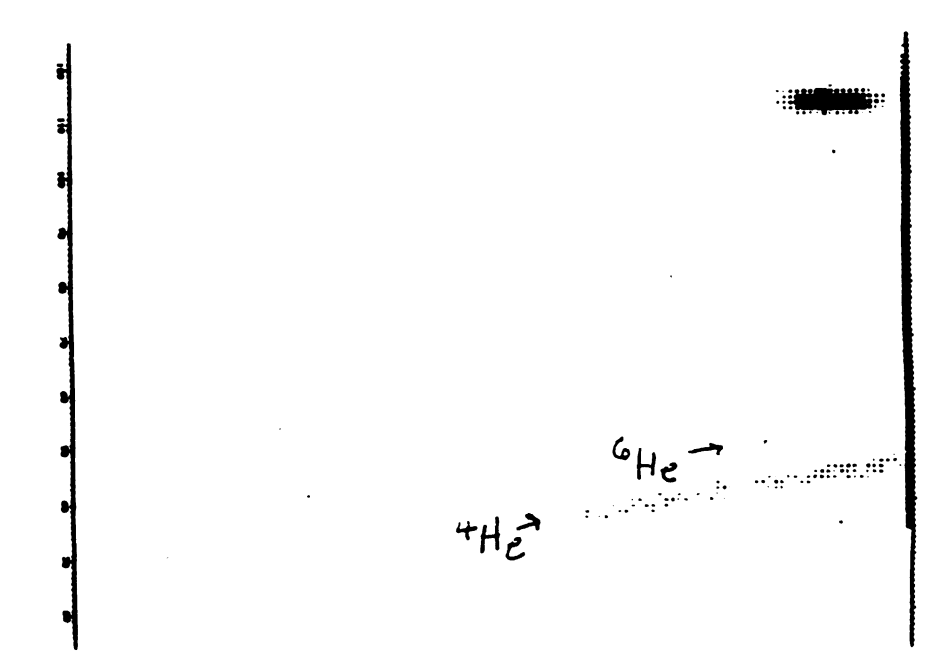


Fig. 27--(a) E_{calc} vs E, BaF₂, Calculated for Z=2, A=6

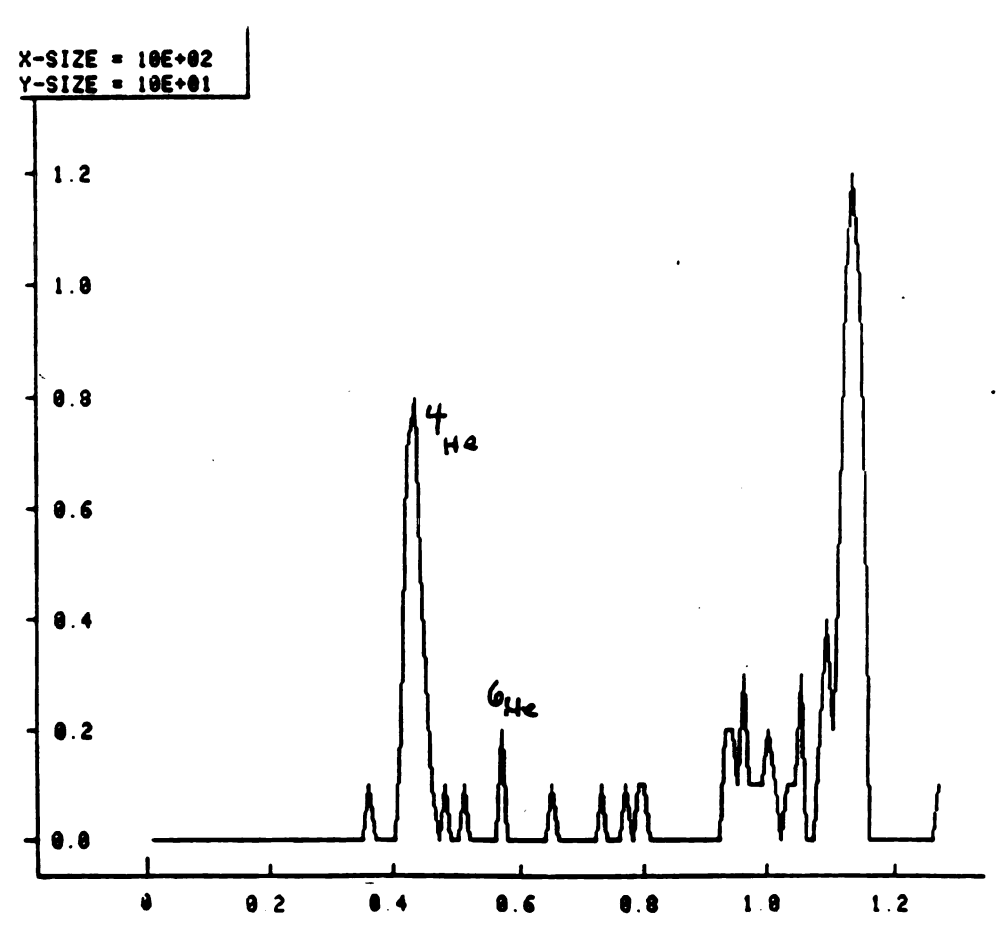


Fig 27--(b) Channel of Best Resolution, BaF₂, Z=2, A=6



Fig. 28--(a) E_{calc} vs E, BaF₂, Calculated for Z=3, A=6

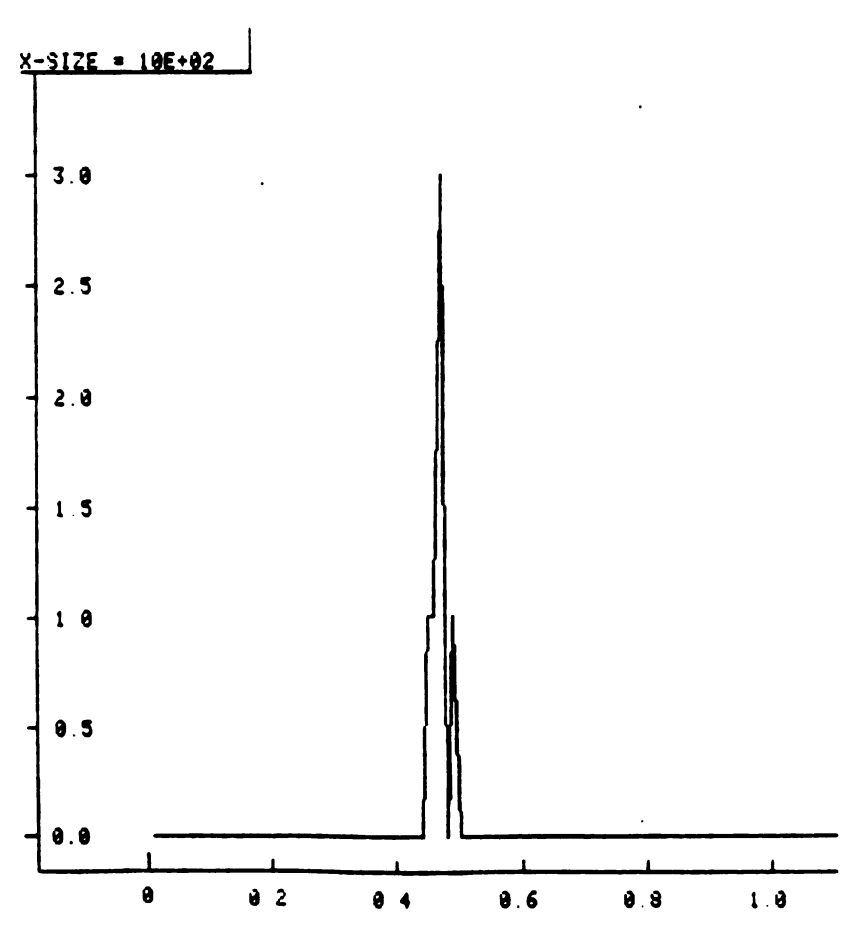


Fig 28--(b) Channel of Best Resolution, BaF_2 , Z=3, A=6

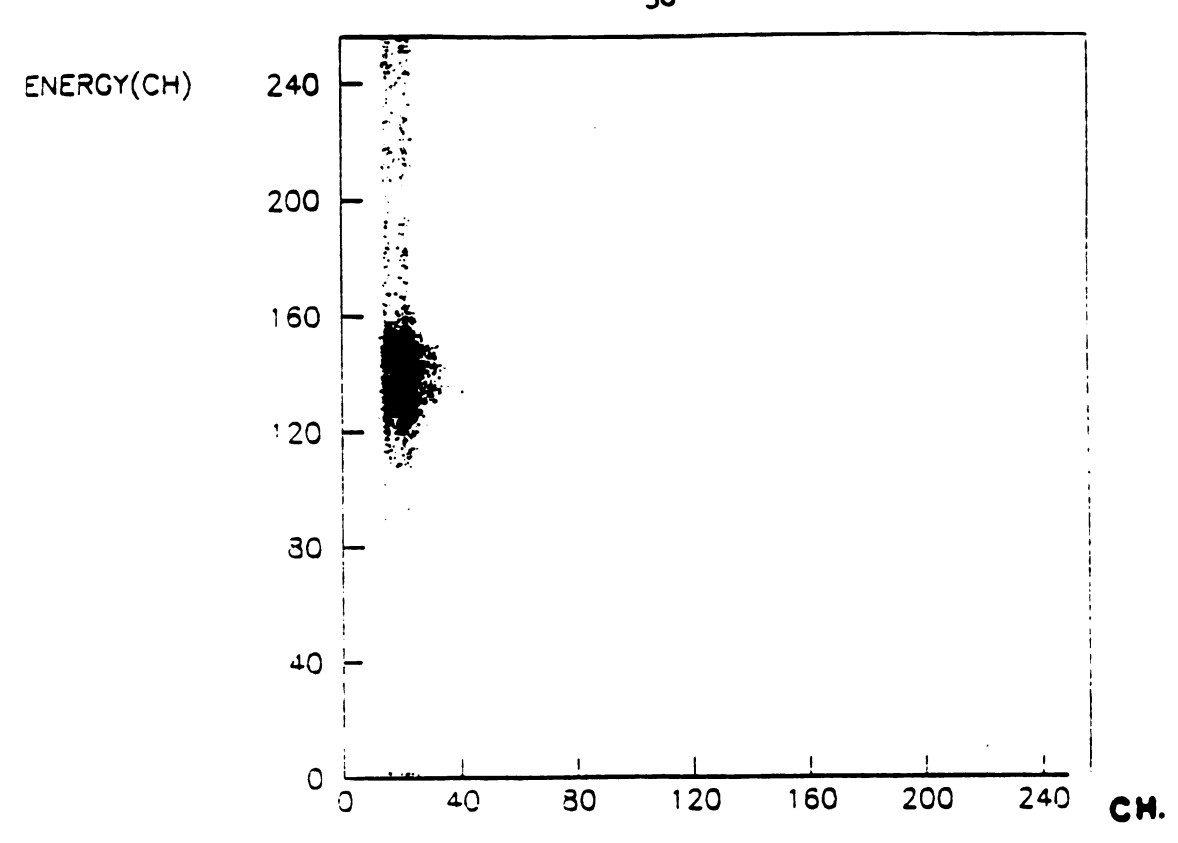


Fig. 29--(a) Ecale vs Zerocross Time, CsI

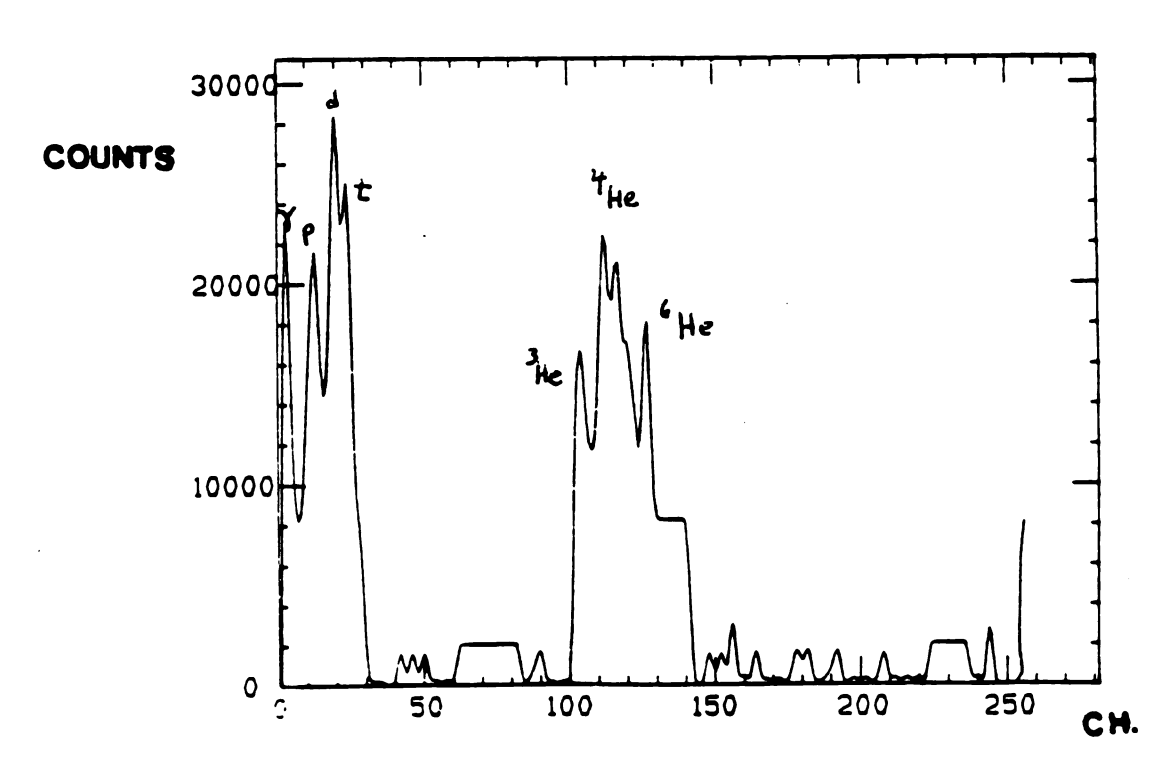


Fig. 29--(b) Projection of Ecale vs Zerocross Time onto Time Axis

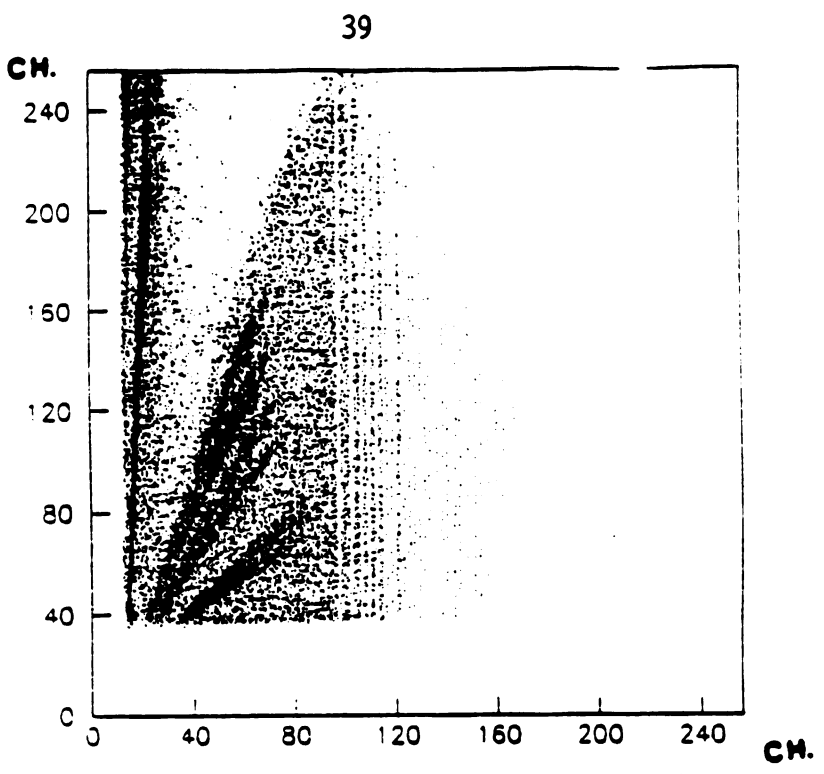


Fig. 30--(a) E_{calc} vs Fast Gate, CsI

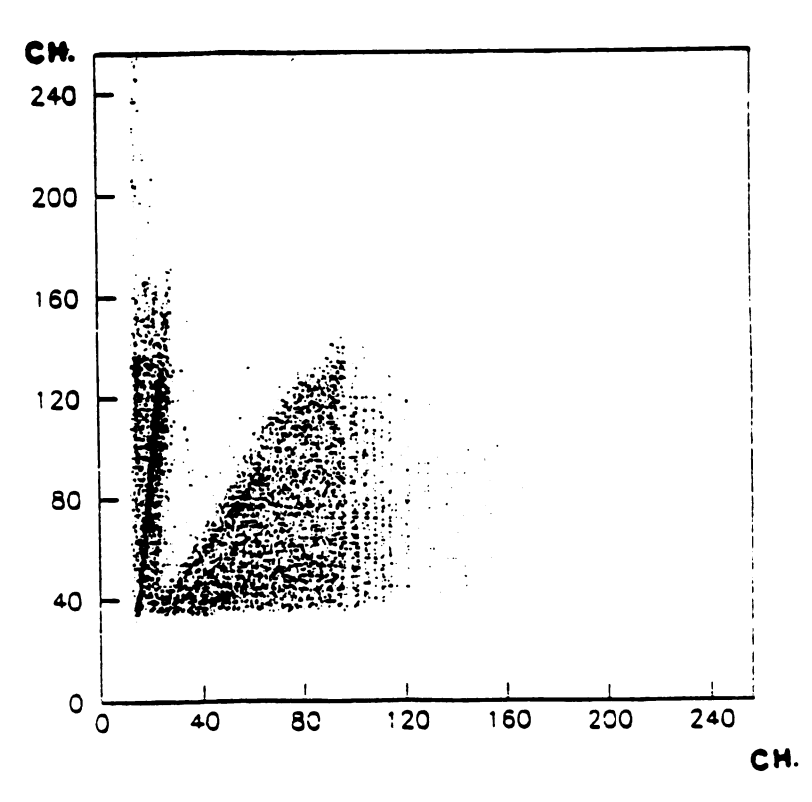


Fig. 30--(b) E_{calc} vs Slow Gate

CONCLUSIONS

The goal of this project was to find a method of particle discrimination for scintillation detectors used in nuclear physics. Of the different methods investigated, the best results were obtained with the final method, using a Si detector coupled with a standard scintillation detector, and comparing the zero-cross time with the energy calculated from the Si dE/dx signal. CsI worked better than BaF₂. However one of the factors influencing the BaF₂ results was that there were fewer overall data points. Perhaps, with better statistics, BaF₂ performance could match that of CsI. Also, time constraints prevented full analysis of the NaI results, which also look promising.

Now that the relationship between dE/dx and E has been calibrated for each (Z<4) isotope in CsI, it is possible to use timing gates for real-time particle discrimination, saving time and effort for both computer and experimenter.

BIBLIOGRAPHY

BIBILIOGRAPHY

¹Birks, J.B., <u>The Theory and Practice of Scintillation Counting</u>, Pergamon Press, Oxford, 1964

²Kasagi, J., Murakami, T., Inamura, T., <u>Use of Charge Integrating ADCs with Pulse Shape Discrimination</u>, Journal of Nuclear Instrumentation in Physics
Research, North-Holland, Amsterdam, 1985, vol. A236, pp.426-427

GENERAL REFERENCES

- Walton, J. T., <u>Designs and Applications of Position-Sensitive Silicon</u>
 <u>Detectors</u>, American Chemical Society -- Division of Nuclear Chemistry and Technology, Annual Conference, Denver, 1987
- Lorenz, E., Mageras, G., <u>Development of a Novel Readout Scheme</u>
 <u>Utilizing Fluorescent Flux Concentrators and Silicon Photodiodes for</u>
 <u>Inorganic Scintillators</u>, ACS Conference, Denver, 1987
- McGrath, R. L., <u>NaI Pulse Shape Discrimination</u>, ACS Conference, Denver, 1987
- Maier, M. Cebra, D. A., Fox, D., Ugorowski, P., Westfall, G., Wilson, D. K., <u>Particle Identification by Pulse Shape Discrimination with Inorganic Scintillators</u>, Acs Conference, Denver, 1987
- Mcguire, C. F., Davids, C. N., Kovar, D. G., Beck, C., Vineyard, M., Prosser, F. W., Reinart, S. V., Kolata, J. J., Kwiatkowski, K., Advances in Light Charged-Particle Detection Using NaI Pulse Shape Discrimination, ACS Conference, Denver, 1987
- Nebbia, G., Fabris, D., Fornal, B., Aatowitz, J. B., Prete, G., Viesti, G., Wada, R., <u>Use of CsI(T1) Scintillators with Photodiode</u> Read-Out in Heavy Ion Experiments, ACS Conference, Denver, 1987
- Sarantites, D. G., Sobotka, L. G., Semkow, T. M., Abenante, V., Elson, J., Nicolis, N., Stracener, D., Valdes, J., Hensley, D. C., "Dwarf Ball": a 4 m Light-Charged Particle Multidetector System for Heavy-Ion Reaction Mechanisms and Spectroscopy, ACS Conference, Denver, 1987
- Hildebrand, K. D., <u>Compact Gas/Plastic Telescopes in Heavy Ion</u> Experiments, ACS Conference, Denver, 1987
- Chan, Y. et al, <u>Position-Sensitive Phoswitch Detectors</u>, ACS Conference, Denver, 1987
- McMahan, M. A., Response of Scintillators to Heavy Ions, ACS Conference, Denver, 1987

